THESIS FOR THE DEGREE OF DOCTOR OF PHILOSOPHY

High Temperature Oxidation and Corrosion of Ni-Based Superalloys for Industrial Gas Turbines

HAIPING LAI
赖海萍

Materials Microstructure
Department of Applied Physics
Chalmers University of Technology
Göteborg, Sweden 2014

High Temperature Oxidation and Corrosion of Ni-Based Superalloys for Industrial Gas Turbines
Haiping Lai
ISBN 978-91-7597-060-8

Doktorsavhandlingar vid Chalmers tekniska högskola
Ny series nr 3741
ISSN 0346-718X

Materials Microstructure
Department of Applied Physics
Chalmers University of Technology
SE-41296 Göteborg
Sweden
Telephone +46 (0)31-7721000

Cover image:
Middle: Gas turbine; Below: The gas turbine blade and a corroded one. The figures surrounding the gas turbine are some images using different instrumental techniques (from left to right): SEM image on cross-section, STEM image, SEM images of non-exposed samples, EDX phase mapping and TEM image as a result of material checking and corrosion investigation.

Chalmers reproservice
Göteborg, Sweden 2014

High temperature oxidation and corrosion of Ni-based superalloys for industrial gas turbines

Haiping Lai
Department of Applied Physics
Chalmers University of Technology

Abstract

High temperature oxidation and corrosion of Ni-based superalloys used for blades in industrial gas turbines was studied using advanced high-resolution electron microscopy methods. Both coated and non-coated alloys were tested.

In the case of alloys covered by protective coatings, the influence of Pt on the material corrosion properties at 900°C was investigated. Due to an extensive research it is known that Pt improves oxidation resistance of coatings above 1000°C. However, the effect of Pt on the oxidation and corrosion resistance at lower temperatures and in the presence of sulphates has not been studied to the same extent. To simulate hot corrosion occurring in gas turbines, a novel method, based on the evaporation of Na_2SO_4 in the furnace was developed. The investigation showed that the presence of Pt improves the protective properties of the coating against oxidation and hot corrosion. The propagation stage of the corrosion on the platinum-free coating was reached already after 100 h of exposure while the scale formed on the platinum-rich coating was thinner and denser, and still appeared to be protective even after 500 h. It was proposed that Pt suppresses the formation of interfacial cavities, degrading the scale adherence by the faster diffusion of Al ions, which can fill the voids.

The performed work on uncoated superalloys includes studies of effects of a) the surface treatment; b) the aggressive environments and c) sulfur in the material on the corrosion properties of the newly developed alloy, SCA425+ and the extensively used alloy IN792. Cyclic exposures up to 260 hours were performed in different atmospheres such as: air, SO_2+O_2+Ar, SO_2+H_2O+Ar and H_2O+O_2. The study showed that due to the relatively high Al content, 10 at.%, SCA425+ might form a protective alumina layer, provided that it receives a surface treatment that creates a zone of defects allowing for a fast enough supply of Al to the metal surface. On the other hand, IN792 does not form a protective oxide scale in any of the investigated conditions and the structure and morphology of the oxide scale are not very sensitive to the surface treatment.

Furthermore, it is shown that the most pronounced effect on the corrosion behavior of the investigated material has the presence of moisture in the atmosphere while the effect of SO_2 up to 260 h exposure seems to be less important. In the presence of water vapor Cr is depleted from SCA425+ due to the evaporation of chromia. The loss of Cr_2O_3 was estimated using a comparison of the Cr depletion in the metal with the amount of Cr_2O_3 in the oxide scale. The results also indicate that the volatilization of chromia slows down with increased exposure. The experiment concerning the influence of sulfur in the material, desulfurization of SCA425+ in hydrogen indicates that S degrades the adherence of the oxide scale.

Keywords: oxide scale, Ni-based superalloys, coating, atmosphere Na_2SO_4, SO_2, H_2O, surface treatment, Pt, electron microscopy.

PREFACE

The research work presented in this thesis was carried out at the Materials Microstructure group at the department of Applied Physics, Chalmers University of Technology, Göteborg, Sweden during the period 2010-2014 under the supervision of Professor Krystyna Stiller. The work was performed in cooperation with the Swedish Competence Center for the study of High Temperature Corrosion (HTC), Siemens Industrial Turbomachinery AB, Westinghouse Electric Sweden AB and Studsvik Nuclear AB.

List of Appended Papers

Paper I. The influence of platinum on the oxidation and sodium sulfate induced hot corrosion of NiAl diffusion coatings
H. Lai, P. Knutsson and K. Stiller
Materials at High Temperatures, **28** (4), November 2011, pp. 302-308.

Paper II. High temperature corrosion of Ni-based alloys SCA425+ and IN792
H. Lai, Y. Cao, P. Viklund, F. Karlsson, L. -G. Johansson and K. Stiller
Oxidation of Metals, **80** (5-6), December 2013, pp. 505-516.

Paper III. A method for investigation of hot corrosion by gaseous Na_2SO_4
P. Knutsson, H. Lai and K. Stiller
Corrosion Science, **73**, August 2013, pp. 230-236.

Paper IV. The effect of surface treatment on the corrosion behavior of Ni-based alloys at 900°C
H. Lai, R. Norling and K. Stiller
In manuscript, 2014.

Paper V. Corrosion kinetics of a single crystalline Ni-based alloy in the presence of water vapor
H. Lai, L. -G. Johansson and K. Stiller
In manuscript, 2014.

Related Paper

Paper VI. Investigation of effects of picking and Fe contents on the corrosion resistance of Ni-based alloy X-750 in BWRs
H. Lai, K. Göransson, C. Gustafsson, J. Chen, Y. Cao, M. Thuvander and K. Stiller
Proceeding to the 16th international conference on Environmental Degradation of Materials in Nuclear Power Systems – Water Reactors, August 11-15, 2013.

My contribution to the papers was the following:

Paper I: I did most of the microscopy work and wrote the paper.

Paper II: I did all the microscopy work and wrote the paper.

Paper III: I did part of the microscopy work and co-authored the paper.

Paper IV: I did all the microscopy work and wrote the paper.

Paper V: I did all the microscopy work and wrote the paper.

Paper VI: I did most of the microscopy work and wrote the paper.

Haiping Lai
Göteborg, September 2014

TABLE OF CONTENTS

CHAPTER 1

Introduction

1.1 Background

As the world's population still increases and countries undergo industrial development and economic expansion, the demand for electricity is very high and will continue to grow. There exist many different energy sources to generate electricity, such as fossil fuel power plants, nuclear power plants and many renewable energy options, however over 80% of the world's electricity is still derived from heat sources [1].

Though the applications of nuclear power plants and many renewable energy options are increasing to generate electricity, the most common way to produce electricity still is the conventional electrical energy generation – due to the fuel flexibility. Over 65% of the world's electrical energy used today is generated by turbines, from burning of fossil fuels, like coal, oil or gas. It is reported that the overall efficiency of a modern fossil fuelled electrical power plant can reach to 60% [1-3]. At the same time, the noxious gases from the combustion processes, resulting in air pollution problems and the carbon dioxide in the air leading to the well-known phenomenon of the greenhouse effect, have become the main environmental issues nowadays. Thus taking both economy and environment into consideration, it is necessary and important to improve the efficiency of electricity generation.

As the most common way to produce electricity from heat source, the conventional electrical generators, like industrial gas turbines, are still far from being capable to be replaced nowadays. The use of industrial gas turbine for generating electricity dates back to 1939. Nowadays, gas turbines have become one of the most widely used power generating technologies [4].

With the increasing demand of electricity and more concerns about the environment, industrial gas turbines are developed to generate power with increased efficiency and lower fuel consumption. The gas turbine efficiency depends on the pressures and the firing temperatures, which can be up to the metallurgical limit set by the material of the turbine blades and the last stage turbine stress level.

The requirements for materials in the hot-gas paths of gas turbines, like the blades/vanes, are very demanding. They need to be capable of operating at very high temperature under both high and fluctuating stresses, and at the same time withstand the severe operating environments. Due to the poor quality of fuels often used in industrial gas turbines, the turbine blades are exposed to hot combustion gases containing contaminants such as a mixture of inlet gases, combusted fuel, sulfur-containing species, water vapor, etc. As a result, the gas turbine materials will not only be oxidized, but could also suffer the more deleterious hot corrosion with the existence of S-containing species. Those impurities in the gas can destroy the protective thermally grown oxide. In order

to prolong the service lifetime of the turbine components under in the highly aggressive conditions, more advanced materials, which withstand not only high mechanical loads, but also surface attacks, are required for hot turbine components.

Nickel-based superalloys are extensively used for hot stage components in industrial gas turbines, due to their good mechanical properties at high temperatures. In the past 60 years, great efforts have been devoted to the development of materials applied in gas turbines by improving the processing methods and optimizing the chemical compositions [5]. For vanes and blades, there has been a gradual move away from conventionally cast Ni-based superalloys towards single-crystal alloys [5]. In the development of power systems, single-crystal Ni-based superalloys are now more and more being applied in industrial gas turbines, as they have better mechanical properties.

The Ni-based superalloys used in the hot components of gas turbines always contain a certain amount of Al and Cr, which can form protective oxides of Al_2O_3 and Cr_2O_3 preventing further removal of the material in the aggressive environments. However, during long-term exposure, the spallation of the oxide layers or evaporation of Cr_2O_3 may occur leading to further depletion of the alloying elements. This finally causes material degradation and will eventually influence the mechanical properties of the alloys.

In order to improve the oxidation and corrosion resistance, and at the same time to preserve the mechanical properties, different coatings enriched in elements forming a uniform, adherent, slow-growing and dense oxide scale, have been applied to Ni-based substrates. Diffusion aluminide coatings are representatives of such coatings. Adding some particular alloying elements will further improve the protective properties of the coatings. One of these elements, known to prolong the life of components, is platinum. The effects of Pt on high temperature oxidation resistance and improvements in the scale adherence of coatings have been presented in numerous studies [6-9]. However, the mechanism of the influence of Pt on the corrosion resistance is not well understood yet. On the other hand, the existence of sulfur as the impurity in alloys will degrade the adherence of the oxide scale. To improve the oxide scale adherence, some methods, like hydrogen desulfurization, are employed to remove the sulfur in the materials [10, 11].

1.2 Scope of the project

This work concerns the high temperature oxidation and corrosion of industrial gas turbine blades. The aim is to understand how the material conditions (structure, composition, surface treatment, etc;) and the environment influence the oxidation/corrosion behavior of the alloy.

More specifically the objectives are:

1. To investigate the influence of minor elements such as Pt and S on the corrosion resistance of the alloy.
2. To study the influence of S and H_2O in the environment on the corrosion resistance of the alloy.

3. To investigate how the surface treatment influences the oxidation and corrosion resistance of the alloy.

Both coated and uncoated Ni-based superalloys were investigated.

CHAPTER 2

Industrial gas turbines

In electric power generation, industrial gas turbines (IGTs) are at the heart of many current power stations, and will play a main role in the growth of electric power capacity from now till 2030 [12]. It is also predicted that IGTs will be more widely applied in the near future, due to the wide variety of fuels that can be utilized and also because the developments of different fuel fired power generation systems are realized into commercial applications. The development of economically viable power systems depends on the high IGTs efficiencies, which demand higher firing temperature. Therefore, in particular the blade materials are required to give acceptable and predictable in-service lifetime in more aggressive environments. Before dealing specifically with the oxidation and hot corrosion-related issues, it is rather necessary to have a brief overview of the working system of gas turbines and the working environments of turbine blades.

2.1 Principle of gas turbines

In principle, compressor, combustor and turbine are the indispensable components of an IGT (Fig. 1). When the gas turbine engines start to work, the surrounding air is sucked in and this incoming air is compressed to a high pressure in the compressor. Then the compressed air is mixed with the fuel, being introduced through an array of spray nozzles, and burned in the combustor to produce high pressure and velocity gas. After leaving the combustion chamber, the hot exhaust gas passes through the turbine and impinges on the blades of the turbine. The consumed heat and gas expansion in the last step are used for the power generation.

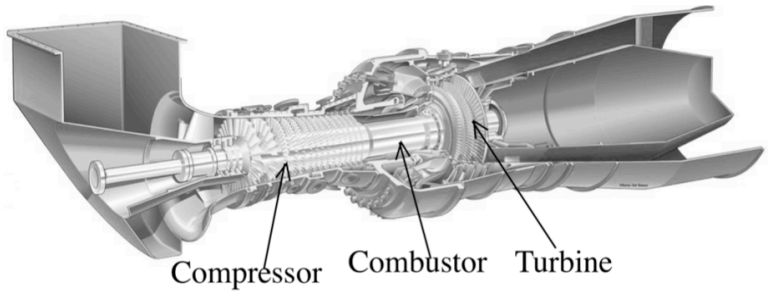

Fig. 1 Section of a stationary gas turbine (From Siemens)

2.2 Operating environments of gas turbine blades

The fuels utilized in IGTs are more diverse today due to the lower cost. The fuel ranges from natural gas to heavy fuel oils and they expand into solid fuels, such as coal, biomass and waste. The contaminants present in the fuel and the air entering the turbine decide the environment within the hot gas path. The combusted gases entering the turbine have the potential to cause deposition, corrosion and erosion damage, depending on the contaminants within them. Sulfur from fuel usually is limited to 0.3% for commercial jet engines and 1.0% for marine gas turbines. Additionally, the aircraft dust can be a source of sulfur and also the intake air contains sea salts, particularly for plants operating within several hundred km of the seacoast. Therefore the combustion of the fuel in the

presence of air or oxygen generates SO_2. On the other hand, the gas turbines generally use large amounts of excess air for combustion, for example, in aircraft gas turbine engines the air-to-fuel ratio ranges from about 40:1 to 100:1. Thus, the gas atmosphere within the hot gas path is highly oxidizing [13] and the use of poor-grade fuels introduces the potential for significant corrosive and erosive damage to gas turbine blades and vanes.

To increase the thermal efficiency, IGTs have been developed to use increasingly higher firing temperatures and pressures, such as temperatures up to ~1400°C at pressures of 30 bar [14]. This will also lead to increased component temperatures. The turbine part of IGTs generally consists of several stages. The high pressure and temperature section is close to the combustor. According to this, the temperatures of hot gas path components - turbine blades, range from 750°C to 1100°C [15]. In addition, the metal temperature over a turbine blade is not uniform and varies from approximately 500°C at the shank to over 1000°C at the hottest part [16]. As a consequence, the requirements on turbine blade materials are more extreme. The materials need to have both good oxidation and corrosion resistance and good mechanical properties, such as creep, fatigue, etc., so that they are able to operate well at temperatures up to 1100°C under high stresses in the aggressive gases.

Gas turbine blades will oxidize in the hot exhaust gases, but generally the oxidation rate below ~900°C is not rapid enough to significantly reduce the service lifetime. However, the presence of salt makes the degradation of materials occurring much easier and more rapidly, therefore it limits the component life. Normally after the sulfur from the fuel reacts with the sodium chloride from air forming sodium sulfate, the sodium sulfate will be carried by the hot exhaust gas and deposit on the hot section components, such as the turbine blades at temperatures below melting point of the salt, causing accelerated oxidation or sulfidation attack. The presence of other sulfates or alkali salts can decrease the melting point of the sodium sulfate, so that salt-induced hot corrosion can occur at much lower stages of turbine blades [17].

In addition to the adverse effect of environmental factors on the material degradation, the cyclic operation way of gas turbines also influences the turbine blade material. Generally in gas turbines, components are often subjected to thermal cycles. Spallation usually takes place during the cooling stages of such thermal cycles. Leading to damage of the protective oxides. When the alloying elements are depleted from the material due to the repeated oxidation and spallation, the components' mechanical properties will also be influenced.

2.3 Turbine blade materials

In order to increase the efficiency of power generation, the gas turbine inlet temperature has been increased to 1300-1500°C, and the lifetime of the highly loaded high-temperature components was required to be extended up to 25000-50,000 h, while the amount of compressor air available for cooling of turbine parts is limited [18]. In addition, the hot exhaust gas produces arduous operating conditions for the hot path components. The resulting problems, such as creep, mechanical fatigue, thermal mechanical fatigue, and also corrosion greatly limit

the service life. Due to material degradation, periodic replacement of hot section components and more support service are required, both of which are very costly.

In the selection of an alloy for turbine blades, except for the consideration of mechanical properties, environmental corrosion resistance is also one of the main important aspects to be considered. The high temperature engineering alloys, mainly based on the transition metals iron, nickel and cobalt, are broadly used, because the oxidation resistance can be improved by adding sufficient amounts of chromium or aluminum to form a protective oxide scale [19].

2.3.1 Nickel based superalloys

The stainless steels were applied as blades and vanes of the first gas turbine engines, but with the development of alloy technology, the excellent high temperature mechanical properties made nickel based alloys replace steels. Ni-based superalloys provide a unique balance of properties to meet the demands of the gas turbines that are subjected to a complex combination of elevated temperatures, high stresses and aggressive corrosion environments. The development of Ni-based superalloys has increased the temperature capability with 700°C over the last 70 years [5].

In general, the air and fuel entering engines in the gas turbines, particularly in land-based turbines, contain certain levels of sodium, potassium, vanadium, and lead. In addition, in biogas there is also a certain amount of H_2S, which will be oxidized to SO_2. These impurities will take part in the sulfidation process and thus lead to corrosion of blade airfoils. Even though the concentrations are quite low, like a few parts per million, these elements can cause destruction of turbine blades in only a few hours [20]. To solve this problem, efforts on two fronts of development are going on. The alloys are being modified to improve the resistance to corrosion attack, and the other effort concentrates on the development of coatings in order to protect the blade alloys from attack.

Development of Ni-based superalloys

During the past 70 years, optimization of the chemical composition together with process development has enabled the performance of the superalloys to be greatly improved. Several different processing methods have been developed since the 1940s for the turbine blades; the wrought materials were replaced by the introduction of cast materials, which later developed further using directional solidification, towards nowadays the single crystalline Ni-based superalloys [5]. Compared to polycrystalline Ni-based superalloys, the fatigue life of the single crystalline alloys are improved due to the removal of grain boundaries. Nowadays, single-crystal superalloys are used in increasing quantities in turbine engines.

Composition, Structure & Phases

The demand on high efficiencies of gas turbines requires the use of firing temperatures as high as possible. Therefore the materials utilized for high temperature components need to have a high melting temperature. In general, the melting temperature of the elements has a close correlation with the atomic number, and the melting point of pure nickel is rather high, 1455°C, which is

advantageous for high temperature applications [5]. At the same time, nickel stays in the FCC form from room temperature up to the melting point. That means there are no phase transformations, avoiding the expansions and contractions that might result in problems for high-temperature components.

Though nickel behaves well and is both tough and ductile, its properties are greatly promoted by the presence of other alloying elements. Thus, to achieve their good performance in the arduous conditions in the gas turbine engine, nickel base superalloys generally have a complex composition. The choice of elements and the amount of elemental constituents included in the Ni-based superalloys are carefully controlled. Except for containing some main elements, like Cr and Al, Ni-based superalloys also contain small amounts of several other elements. In Fig. 2, the partitioning of important elements are shown, and it can be seen that the elements can be grouped into 3 important classes: γ − forming elements, γ' − forming elements and grain boundary elements.

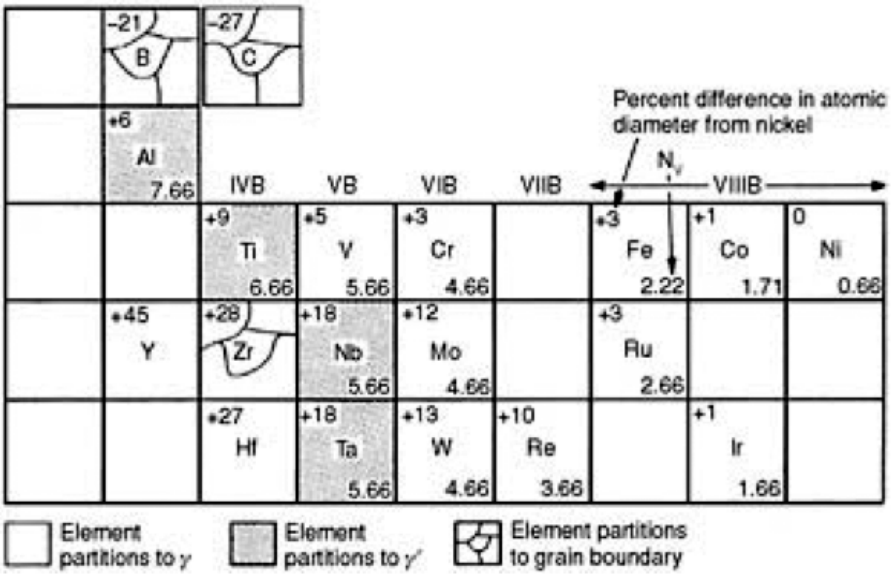

Fig. 2 Partitioning of elements in Ni-based superalloys [5, 20]

γ - forming elements: The γ phase exhibits FCC structure, and in general, it forms a continuous matrix phase with other phases residing inside it. The elements composing the γ matrix mainly come from Group V, VI and VII, which are cobalt, iron, chromium and some refractory metals, like molybdenum and tungsten [5, 20, 21].

γ' - forming elements: The γ' forms as a precipitate phase with FCC structure and is observed as spherical or cuboidal particles, depending on the extent of matrix-lattice mismatch. The elements partitioning to γ' mainly belong to Group III, IV and V (marked as grey in Fig. 2), such as Al, Ti, Nb and Ta. γ' in matrix γ can form A_3B type compounds, and elements like nickel, cobalt or iron constitute A, while alloying elements such as aluminum, titanium or tantalum constitute B. The γ' precipitates are coherent with the matrix and contribute to the strength of the precipitation-hardened alloys.

Grain boundary strengthening elements: The elements from Groups II, III and IV, like boron and carbon, tend to form borides and carbides and segregate at grain boundaries [5, 20-23]. It should be emphasized here that the grain boundary strengthening elements are favored in polycrystalline alloys, but they are suppressed in single crystalline materials.

Single crystalline Ni-based superalloys

Alloys might be improved by adjusting their composition, however they can also be improved by innovations in processing, such as directional solidification or single crystal technology. Unlike the polycrystalline alloys, the single crystalline alloys are free from grain boundaries. The lack of grain boundaries leads to an increase in the incipient melting temperature and therefore it helps to get fine-scale precipitation of γ' when heat treated in the temperature range 1240 – 1330°C [24]. In the applications for gas turbine blades, the lack of grain boundaries improves the creep and fatigue performance in service [25, 26].

The single crystal casting technology was developed about 30 years ago, and since 2000, the fourth-generation single-crystal superalloys have emerged [5, 27]. A typical microstructure comprises a multitude of γ' cuboidal precipitates in a γ matrix. Fig. 3 shows cuboidal γ' precipitates in a γ matrix of SCA425+ alloy.

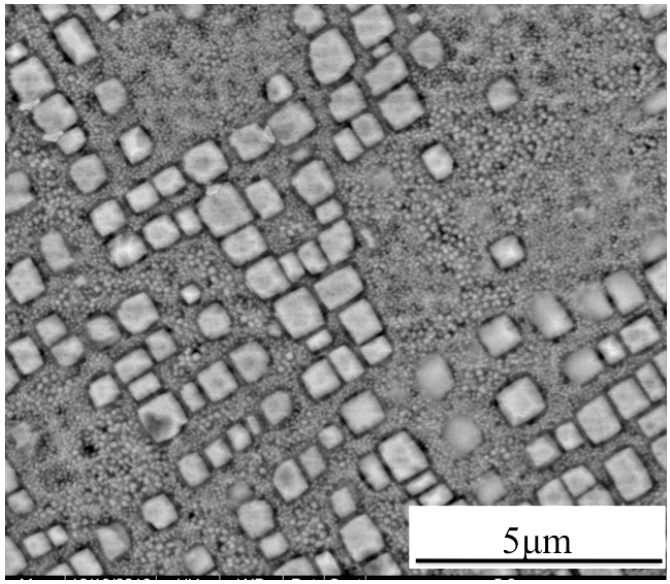

Fig. 3 Scanning electron micrograph of a two phase γ – γ' microstructure of single crystal Ni-based superalloy SCA425+

2.3.2 Coatings

In general, Ni-based superalloys containing low chromium and aluminum content are not qualified to resist oxidation and corrosion for long-term operation in gas turbine environments. Therefore, different types of coatings are employed for gas turbine components to improve the oxidation and corrosion properties of the alloys. It is reported that coated turbine blades have service life 2 to 5 times longer than their uncoated counterparts [13, 15].

Diffusion coatings

As the earliest coatings used from the late 1950s, the diffusion coatings are still in wide and active use today [19]. This is due to the lower cost and various well developed processing techniques, such as slurry cementation, powder pack cementation and chemical vapor deposition (CVD) [28]. Diffusion coatings are formed by enriching the surface with aluminum, chromium or silicon. Aluminum diffusion coatings are one of the most common and popular diffusion coatings used in industry nowadays. They are widely used to protect different components in gas turbines against oxidation at high temperature, and provide a protective thermally grown oxide (TGO) for the underlying substrate. In addition, they could also act as bond coatings for thermal barrier coatings (TBCs). For both applications, the aluminum diffusion coatings can perform very well. They form a thin and adherent oxide scale with excellent metallurgical bonding to the underlying substrate, and show diffusion stability with the substrate and notable resistance to erosion and corrosion, etc..

The protectiveness of aluminide coatings relies on the high content of aluminum at the surface of the diffusion coatings, promoting selective oxidation of aluminum. The aluminide layer may grow outwards or inwards, and this depends on the type of coating and the selected process parameters, etc. [12]. However, no matter what kind of method is used, the main goal with aluminide coatings is to achieve the formation of an outer layer (such as β–NiAl) capable of forming a protective Al_2O_3 scale.

Influence of Pt in the alloys

Our previous studies by Angenete and Svensson have shown that addition of Pt enhances coatings' performance by improving oxidation and corrosion properties. Pt suppresses the amount of Ni and Co and allowed a high amount of Al at the surface [29]. It was also found that Pt suppresses the formation of Ni-rich oxides and improves the selective oxidation of Al to form α-Al_2O_3. Platinum affected the formed oxide scale without directly participating in the reactions [30, 31]. Moreover, platinum modification has been shown to reduce the sensitivity to sulfur by suppressing the formation of voids at the oxide/metal interface, i.e. by improving the oxide adhesion and therefore improving the oxidation resistance [6-9, 32, 33]. Recently it was also reported that the addition of a small amount of Pt (<10at.%) to Ni_3Al alloys improves Type I hot corrosion at 900°C, because Pt has positive effect of decreasing the extent of oxide scale fluxing when the surface is covered by fused Na_2SO_4 [34].

In order to form Pt modified nickel aluminide coatings, a layer of Pt, typically 6 μm thick, is first deposited, either by electrodeposition or by ion plating. Following a post coating annealing process, to diffuse the platinum to the substrate, aluminizing gives rise to the Pt modified NiAl coating [35, 36]. In this work, it is shown that with Pt in the coating, more protective oxide is formed even in corrosive environments, like in the presence of Na_2SO_4, and the propagation stage was avoided.

Influence of sulfur in the alloys

It is known that sulfur present as impurity in nickel-based alloys can segregate at high temperature to the free metal surface [37]. Thus, when the alloy is exposed to the oxidative or corrosive environment, sulfur will segregate to the voids, which are formed at the metal oxide interface, and stabilize the void surface by decreasing the metal surface energy. This will degrade the adherence of the oxide scale [10, 37-39]. One of the possibilities to prevent such a degradation is achieved by the addition of reactive elements, like yttrium, to tie up sulfur in the alloy [11]. Presence of Pt in the alloy showed also to have a beneficial effect in that respect since this element seems to prevent the void formation. Finally the amount of sulfur in the material can be minimized by hydrogen desulfurization or repeated oxidation and surface removal to gradually deplete the alloy of its sulfur content [10, 11, 40, 41].

CHAPTER 3

Oxidation and corrosion

When alloys are used at elevated temperatures, they are undergoing inevitable oxidation and in some cases the formed oxide is protective so that further degradation of the material will be stopped or slowed down. However, if the working environment is too aggressive for the material, corrosion will take place. Of course, designers in industry would prefer if corrosion could be completely avoided and a lot of efforts have been put to improve corrosion properties, in different ways. The morphologies and types of oxides or corrosion products are greatly influenced by the environment. Commonly in industrial gas turbines blades, chromia, alumina, even sulfides, etc., form due to the very oxidizing hot exhaust gases, which also carries some impurities. Thus, understanding of the corrosion mechanisms in different environments will help to reduce the occurrence of corrosion.

3.1 Oxidation theory

When alloys are used in oxidizing environments, an oxide scale will form. The formation rate and the properties of the oxides determine whether the oxide scale is protective or not. In general, a protective oxide should be thin, dense, slowly growing, adherent to the metal, and thermodynamically stable within the working temperature range.

3.1.1 General formation of metal oxides

When a clean metal M reacts with oxygen gas, the oxide M_aO_b forms, and it can be expressed as:

$$aM(s) + (b/2)O_2(g) \rightarrow M_aO_b \qquad (3.1)$$

Not all oxidation reactions can occur, which is decided by the free energy change associated with the formation of the oxide. Only when the free energy change of the reaction, ΔG, from the reactants to products is negative, the reaction 3.1 from left to right occurs spontaneously [42].

The initial stages of reaction between the metal and oxygen are shown in Fig. 4. Initially, oxygen is adsorbed at the metal surface. As the reaction proceeds, the oxygen starts to dissolve in the metal. After that, either a film of oxide or separated oxide islands nucleate on the surface. When a continuous oxide film of M_aO_b forms, it becomes a barrier separating the metal and the oxidizing environment. Then further oxidation can only proceed by solid-state diffusion through the oxide film. However, it might also form porous oxide scales, which do not become the solid-state diffusion barrier between the reactants, because the pores in the scale provide more paths for the transportation of metal and oxygen ions. Due to the high mobility of oxygen ions, the oxidation becomes much more rapid, and it cannot be slowed down unless a new barrier is built-up forming a dense and stable oxide layer.

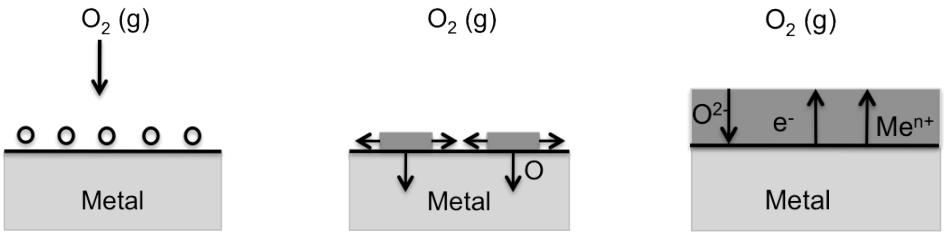

Fig. 4 The initial stages of formation of oxide scale: (1) adsorption of oxygen, (2) oxide nucleation and oxygen dissolution and (3) formation of oxide scale [43].

3.1.2 Solid-state diffusion mechanism

When a dense oxide film is formed, the reaction may be preceded by solid-state diffusion of oxygen or metal ions through the scale. The diffusion and transport of the ions rely on the presence of imperfections or defects in the oxide. Based on the different defects, the diffusion mechanisms can be sorted into bulk diffusion (also called lattice diffusion) and short-circuit diffusion.

The defects are divided into three main groups: point defects, line defects and plane defects. The point defects are responsible for lattice diffusion, while the short-circuit diffusion is mainly due to the existence of line and plane defects. However, the relative contributions to scale growth by bulk or grain-boundary diffusion will depend on the temperature and the oxide grain sizes [44].

Point defect structures in oxides and lattice diffusion

Simple point defects include (i) empty sites or vacancies at the position of constituent atoms in the structure and (ii) interstitial atoms in the interstices between the regular sites. For the metal oxides, in principle, there are two groups of point defect structures: stoichiometric defect structures, in which complementary point defects are formed to conserve the balance between M (metal) and O (oxygen) atoms, and non-stoichiometric defect structures, which always have a deficit of O or M relative to the stoichiometric composition.

Stoichiometric defect structures: The two most common defect structures in stoichiometric crystals are termed Schottky and Frenkel defects, respectively. The Schottky defect contains equivalent concentrations of anion and cation vacancies (V_O and V_M) in the structure. This type of disorder involves defects in both the anion and cation lattices, such as in Fig. 5a, where doubly charged oxygen and metal vacancies $V_O^{2\bullet}$ and $V_M^{2'}$ are present. The Frenkel defects, on the other hand, are either in the cation or in the anion lattice. As shown in Fig. 5b, the Frenkel defect pair involves vacancies and interstitial atoms of the same component (like $V_M^{''}$ and $M_i^{\cdot\cdot}$) and in equivalent concentrations.

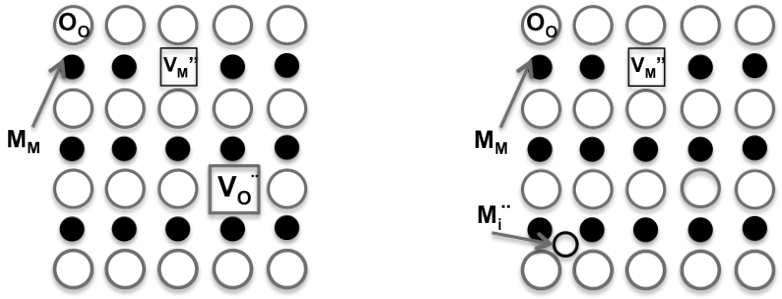

(a) *(b)*

Fig. 5 (a) Schottky defect and (b) Frenkel defect in an oxide MO.

Non-stoichiometric defect structures: The non-stoichiometric defects are more common in metal oxides and have either metal excess or metal deficit, which leads to that the predominant defects are metal interstitial ions or vacancies. The defect structures in metal oxides are summarized in Fig. 6. When the oxide has metal excess, e.g. $M_{1+y}O_2$, the interstitial metal ions dominate. Alternatively, if the oxide is deficient in oxygen, e.g. MO_{2-x}, there will be oxygen vacancies in the structure. If such types of defect structures are charged, they will have a positive net charge, which will be compensated for by the formation of an equivalent amount of negative electronic defects. Thus, such oxides are n-type semiconductors. On the other hand, the non-stoichiometric oxides with a metal deficit, like $M_{1-y}O_2$, or oxygen excess, e.g. MO_{2+x}, have metal vacancies and oxygen interstitials as dominating defects, respectively. Such non-stoichiometric oxides belong to p-type semiconductors [44, 45].

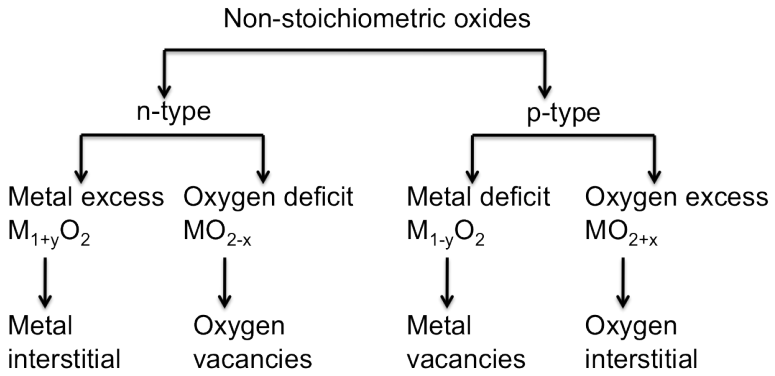

Fig. 6 Summary of non-stoichiometric defects of metal oxides.

Linear and planar defects and short-circuit diffusion

Linear defects refer to displacements in the periodic structure in certain directions. The planar defects are mainly stacking faults, internal surfaces, like grain boundaries, and external surfaces. The diffusion along line and surface defects requires smaller activation energies than lattice diffusion, typically only 50 – 70% of the activation energy of lattice diffusion. In addition, the diffusion coefficients are 10^4 – 10^6 times larger than lattice diffusion coefficients [43]. This type of diffusion is often termed short-circuit diffusion and the defects are called high diffusivity paths, due to the rapid diffusion provided by grain boundaries, surfaces, cracks and so on. In general, at low temperatures, the short circuit diffusion is dominant, while at high temperatures the diffusion mechanisms are either lattice diffusion and/or short-circuit diffusion.

3.1.3 Basic oxidation kinetics

The oxidation kinetics can be described by measuring weight gain or oxide thickness. In general, the oxidation kinetics comprises three common oxidation behaviors: parabolic, logarithmic and linear, see Fig. 7.

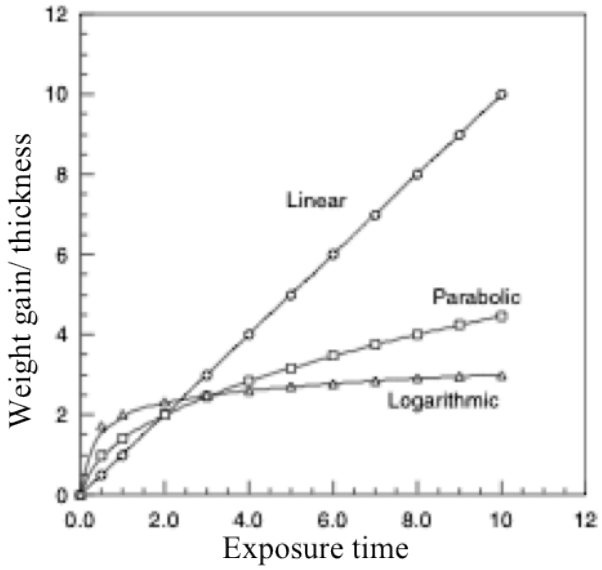

Fig. 7 Weight gain or oxide thickness for the kinetic laws of metal oxide growth [42].

Parabolic oxidation

At high temperature, the oxidation rate of most metals follows the parabolic kinetic law, see Fig. 7. In such an oxidation growth mode, the square of the oxide thickness is proportional to the time t:

$$x^2 = k_p t \qquad (3.2)$$

Where k_p is the parabolic rate constant, t is the exposure time and x is the mass gain or the oxide thickness [42]. To use the mechanism of parabolic growth, the following conditions must be fulfilled:

1. The oxide layer is compact and perfectly adherent.
2. Migration of ions through the oxide layer is rate controlling.

In general, the parabolic law is applied to analyze high-temperature oxidation kinetics, where the reaction rates are controlled by diffusion through relatively thick oxide scales.

Logarithmic oxidation

At lower temperatures, the formation of thin oxides usually obeys the logarithmic law:

$$x = k_e \log(at+1) \qquad (3.3)$$

Here k_e is the rate constant of the logarithmic process, x is the oxide thickness, t is the time and a is a constant. At low temperatures, the oxidation rate is often logarithmic in thin oxides, but when the oxide becomes thicker the parabolic kinetics usually takes over.

Linear oxidation

Unlike the parabolic and logarithmic oxidations, the oxidation rate does not change with time in this case. A linear oxidation can happen at quite early stages

of oxidation, when the thin oxide films are not protective. However, the linear oxidation kinetics can also be observed when thick oxides are formed, e.g. the oxidation reaction at the scale/metal interface often follows the linear kinetics. In addition, if micro cracking or porosity occurs in thick scales, the oxidation kinetics might be transformed from parabolic to linear. Such cases are very common when a protective film breaks down at a continuously increasing number of sites, resulting in an increased oxidation rate, which is called breakaway. Linear oxidation can be expressed as follows:

$$x = k_l t + C \quad (3.4)$$

where x is the oxide thickness, k_l is the linear rate constant, t is the exposure time and C is the thickness at the onset of linear growth [42, 46].

3.1.4 Oxidation of alloys

Commercial high temperature alloys contain a number of alloying elements to achieve desirable mechanical properties. Such alloy components have different affinities for oxygen and do not diffuse at the same rate in the oxide or the alloy. Consequently, the simple kinetic rate equations often do not apply, and the scale and alloy compositions change in a complex way with time. The second component may enter the scale, affecting its structure, or may accumulate as metal or as oxide beneath the main scale. Also, if oxygen diffuses into the alloy, precipitation of the oxide of the less noble metal may take place as internal oxide.

Chromium and aluminum are the important alloying elements for the material used in high temperature applications because the growth rates of Al- and Cr-oxides are slow and the formed scales are considerably more stable than the other oxides, such as NiO.

Oxidation of chromia forming Ni-based alloys

One of the purposes of the addition of Cr to Ni-based alloys is the formation of a protective Cr_2O_3 scale. Cr_2O_3 (Escolaite), subsequently referred to as chromia, is the only solid chromium oxide that is thermodynamically stable at high temperature. It has the corundum structure, very low non-stoichiometry and low ionic conductivity [43]. At high temperatures (>1000°C), Cr_2O_3 can be oxidized and transfer to the volatile CrO_3 [43].

In Ni-based superalloys, initially Ni-containing oxides are formed together with Cr_2O_3. Thus, before a continuous chromia layer is built up, a reaction between Cr_2O_3 and NiO, forming $NiCr_2O_4$ spinels takes place [44, 47]. Since the cation diffusion is much slower through the $NiCr_2O_4$ spinels than it is through NiO, the spinels can act as a barrier for an outward diffusion of Ni ions and the total Ni flux through the oxide scale will decrease. However, since the growth rate of Ni-containing oxides is much faster than for Cr_2O_3, a large amount of $NiCr_2O_4$ and NiO can form before a continuous Cr_2O_3 layer is created. This phenomenon is called “transient oxidation”. The extent of the period for transient oxidation depends on the Cr content in the alloy and the oxygen pressure.

In most applications, the ambient oxidizing atmosphere contains also water vapor. Thus, the effect of moisture on the oxidation/corrosion process of Fe-based alloys has been studied in a number of works [45, 47-51]. It has been

shown that in the case of Cr_2O_3, water vapor promotes chromium volatilization, according to the following reaction:

$$½\ Cr_2O_3(s) + ¾\ O_2(g) + H_2O \rightarrow CrO_2(OH)_2(g) \qquad (3.5)$$

This means that the reactive evaporation of chromia (see above) is more pronounced in a moist atmosphere, which degrades scales in the long term. Moreover, the rapid depletion of chromium due to the water vapor may affect the selective oxidation of elements or the formation of oxides. For example, in the Fe-Cr systems, the protective $(Fe_{1-x}Cr_x)_2O_3$ converts to FeCr spinel oxides in the presence of water vapor [52]. However, the effect of H_2O on the corrosion resistance of Ni-based alloys is less well investigated and there are still some debates in this matter.

Oxidation of alumina forming Ni-based alloys

In general, alumina formers have better high-temperature resistance than their chromia-forming counterparts. This is because the transport of reactive species through alumina is inherently slower than through chromia. Furthermore, alumina unlike Cr_2O_3 does not suffer from volatilization at the temperatures above 1000°C, and therefore alumina-forming alloys can be used at higher temperatures [53-55].

During the oxidation of alumina-forming alloys, like NiAl, Al_2O_3 can be formed in different crystallographic phases. At lower temperatures or in the early stages of oxidation, the metastable oxides γ-Al_2O_3, δ-Al_2O_3 and θ-Al_2O_3 are often formed. These alumina phases contain high concentrations of cation vacancies. After longer oxidation they can transform to α-Al_2O_3. Due to the nearly perfect stoichiometry, α-Al_2O_3 exhibits low diffusivities for cations and anions as well as being highly stable. Therefore the formation of mature α-Al_2O_3 scales reduces the oxide growth rate. The transformation sequence from metastable alumina to the stable α-alumina phase, depending on temperature, can be expressed as the following [56-58]:

$$\gamma \xrightarrow{700°–800°C} \delta \xrightarrow{900°–1000°C} \theta \xrightarrow{1000°–1100°C} \alpha\text{-}Al_2O_3$$

Transient alumina

The existence of δ- or θ-Al_2O_3 scale on NiAl following high temperature oxidation is not widely reported, because these phases appear only after short exposures and at relatively low temperatures. In most other cases the stable α-Al_2O_3 is formed. The Al_2O_3 structures (the details about the crystal structures can be found in Table.1) can be divided into two categories: face-centered cubic (fcc) and hexagonal close-packed (hcp) arrangements of the oxygen anions. The stacking sequence of oxygen anions in metastable Al_2O_3 is by the way of …ABCABC…, while Al cations mainly occupy tetrahedral and octahedral sites [56, 58]. Transient alumina contains high concentrations of vacancies and lattice defects, resulting in oxide growth by outward diffusion of aluminum cations.

Al_2O_3 Phase	Crystal system	Lattice parameters (Å)	Oxygen sub-lattice	Type of occupied vacancies
γ - Al_2O_3	Cubic	a=7.911	fcc	Octahedral and tetrahedral
δ - Al_2O_3	Tetragonal	a = 7.96 c = 11.7	fcc	Octahedral and tetrahedral
θ - Al_2O_3	Monoclinic	a = 5.64, b = 2.92, c = 11.83, β = 104°	fcc	Octahedral and tetrahedral
α - Al_2O_3	Rhombohedral Hexagonal	a = 4.7589 c =12.991	hcp	Octahedral

Table. 1 Crystal structure of the main alumina phases [59].

α -alumina

α-Al_2O_3, which has a corundum structure, is the most stable alumina phase, and it is formed by irreversible transformation from the metastable phases. Due to the large band gap and high lattice energy, the concentrations of ionic and electronic defects are extremely small [43]. Therefore the perfect stoichiometry and stability of α-Al_2O_3 help to make it an important constituent of many protective oxide scales formed on the surface of high-temperature metals and alloys. The stacking sequence of the oxygen ion planes is …ABAB…, and the Al ions occupy 2/3 of the octahedral positions. α-Al_2O_3 grows mainly by diffusion of oxygen along grain boundaries, because of the high density and the low amount of lattice defects.

It has been reported that the addition of platinum can reduce the spallation of alumina scales [7]. One of the proposed reasons is that Pt delays the transformation from transient alumina to α-Al_2O_3. This helps to relax stresses caused by the rapid volume change [7, 60]. But this explanation was not supported by our research. In our previous work, it was found that the beneficial effect of Pt is to prevent the formation of interfacial voids and to promote filling of created cavities with the oxide.

3.2 High temperature corrosion

In industrial processes, in addition to oxygen, the materials are also exposed to more aggressive environments, which contain mixed gases, molten salts, like alkali and sulfates, fly ashes and so on. At high temperatures, the interaction of these constituents with components results in accelerated oxidation or sulfidation attack. This refers to high temperature corrosion or hot corrosion, which leads to a rapid degradation of materials.

3.2.1 Characteristics of hot corrosion

The three basic kinetic oxidation laws, described in 3.1.3, are also applicable for high temperature corrosion. The main difference is that the addition of salts makes the working environments more complex and usually the degradation becomes accelerated. In general, based on the temperature range and the microstructure formed, hot corrosion can be divided into two main types: high-

temperature hot corrosion HTHC (Type I) and low-temperature hot corrosion LTHC (type II).

High temperature hot corrosion (HTHC)

In general, high temperature hot corrosion occurs in the temperature range of 750–950°C. In this corrosion mode, both incubation and propagation periods are included. The corrosion starts from the alkali metal salts, like Na_2SO_4, which have very high thermodynamic stability, condensing on the surface. Initially the salt attacks the protective oxide film and further progresses to reach the metal. Chromium in the substrate material will be depleted, therefore the oxidation of the base material accelerates and a porous scale starts to form. In addition, sulfides form underneath the protective oxide in this form of corrosion. This might lead to catastrophic consequences because these sulfides can be molten in the HTHC temperature range. In the case of HTHC, usually a porous non-protective external oxide scale with internal oxides underneath is observed, and at the same time, there is a chromium depletion zone and internal sulfidation below the oxide scale [44].

Low temperature hot corrosion (LTHC)

The low temperature hot corrosion is observed within the temperature range of 650–850°C. In this form of hot corrosion, the temperature is lower than the melting temperature of most salts, so the salts will deposit on the oxide or metal surface and react to form base metal sulfates, and this leads to local pitting. Then these sulfates together with the alkali metal sulfates form low melting point eutectic mixtures, which prevent formation of a protective oxide. Different from HTHC, LTHC requires a high partial pressure of SO_3 in the gaseous phase to make the reaction occur. In contrary to HTHC, in LTHC there is neither an incubation period nor sulfidation or chromium depletion. Typical features in this type of corrosion are the existence of pitting, little internal oxidization, no internal sulfides and no depletion zones [44, 61, 62].

3.2.2 Mechanism of hot corrosion

The hot corrosion of alloys can be divided into two steps: first, an initiation stage in which the corrosion rate is low and similar to the high temperature oxidation in the absence of deposits, and, second, a propagation stage in which large amounts of depletion in Al or Cr lead to rapid or catastrophic corrosion.

In the case of HTHC, initially the oxygen coming from Na_2SO_4 or the gas environment reacts with the metal. The reaction product separates the deposit and the alloy surface, and the exhibited feature is quite similar to the gas-alloy reaction without the deposits. However, the failure of the protective oxide layer, due to thermal stresses, chemical reactions, etc., allows sulfur from molten salts to access the substrate metal. The propagation stage of hot corrosion mainly occurs because the molten deposits destroy the protectiveness of the oxide scales. Goebel and Pettit have proposed two possible propagation modes: basic and acidic fluxing of the protective oxide scale [63, 64]. Basic fluxing occurs when the oxide ions O^{2-} from the molten salts and from the oxide form soluble species (anions). In the basic fluxing, sulfur from Na_2SO_4 is usually found to form metal sulfides in the alloy substrates or in the corrosion product. In addition, the amount of attack is determined by the oxide ions in the molten salts. When the

oxide ions reach to the saturated concentrations in the molten salt, the hot corrosion will be restricted by the temperatures, which influences the ions diffusion rate and the thermal stabilities. Compared to basic fluxing, acidic fluxing leads to much more severe oxidation. It takes place by the decomposition of oxides into the corresponding cation and O^{2-}. Especially when elements like molybdenum and vanadium in the alloys cause deposits, the formed oxides such as Al_2O_3, Cr_2O_3 or NiO will dissolve into the metal in the local region. Thus the protective oxide scale will be destroyed. Furthermore, a large amount of Al or Cr will be depleted, which could make the alloy lose the ability to form protective oxides.

In the case of LTHC, it also takes place in two stages: (1) liquid sulfate forms on the surface, (2) propagation attack takes place by inward migration of SO_3 and outward transport of metal elements through the liquid salts.

Corrosion of NiAlCr alloys in Na_2SO_4 gases

As shown in the present work, when the exposure temperature is above the melting point of Na_2SO_4 (884°C when it is pure), it will be present in the state of gas. At the initial reaction, a thin film of Na_2SO_4 will be absorbed on the surface as a monolayer [65]:

$$Na_2SO_4\ (g) \rightarrow Na_2SO_4\ (ads) \qquad (3.6)$$

The absorbed Na_2SO_4 could react with the formed oxides, like Cr_2O_3 and Al_2O_3 [66]:

$$Cr_2O_3(s) + {}^1/_2O_2(g) + 2Na_2SO_4(g) \rightarrow 2Na_2CrO_4(s) + 2SO_2(g) \qquad (3.7)$$

Therefore, the protective Cr_2O_3 is converted to chromate ions in the sulfate by consuming the oxide ions from Na_2SO_4. The Cr_2O_3 is not stable any more since the oxide ion concentration of Na_2SO_4 is sufficient to form chromate ions. At the same time, the oxidation of chromium from the sulfate-coated alloy is accelerated by the oxygen ions from the salt. Then the oxide ion activity of Na_2SO_4 is reduced, which leads to an increased sulfur activity in Na_2SO_4. Therefore sulfur enters the alloy by diffusion through the oxide scale to form chromium sulfide.

Consumption of chromium will be reduced with the formation of protective alumina. Normally, Al_2O_3 is stable in the presence of Na_2SO_4, but still the reaction between Na_2SO_4 and Al_2O_3 can take place and is a little bit more complicated. The reaction is influenced by the oxygen and SO_3 pressures, and is defined by the equilibrium Na-S-O system. The Na_2SO_4 can react with Al_2O_3 and form different phases, like $NaAlO_2$ or Al_2S_3, depending on the SO_3 and O_2 pressures. The formation of $NaAlO_2$ causes dissolution of Al_2O_3 by the oxide ion-enriched Na_2SO_4 and then the protective Al_2O_3 is destroyed. The reaction is expressed as follows [66]:

$$Na_2SO_4(l) + Al_2O_3(s) \rightarrow NaAlO_2(l) + SO_3(g) \qquad (3.8)$$

Corrosion in sulfur containing gases

Combustion of sulfur containing fuels leads to the formation of atmospheres that contain SO_2+O_2 and/or SO_3. The reactions of metals and alloys with sulfur are governed by the same basic principles as for metal-oxygen reactions. But for most metals, sulfur is a more aggressive oxidant than oxygen. Thus, the

commonly used metals such as iron, nickel and cobalt or their alloys containing chromium and aluminium exhibit reaction rates in the sulfur-containing environments that are much faster than in oxygen, see Table. 2. The high reaction rates of metals in sulfur is due to the high concentration of point defects and higher deviations from stoichiometry in the sulfides, leading to much faster diffusion in sulfides than in the corresponding oxides [43, 67]. Furthermore, sulfides are thermodynamically less stable thermodynamically and melt generally at lower temperature than the corresponding oxides [67].

Table. 2 Parabolic rate constants k_p or oxidation and sulfidation of some metals in O_2 and S-containing gas [43].

Reacting gas	K_p(g/(cm^{4}s)			
	Ni	Co	Fe	Cr
O_2	9.1×10^{-11} (1000)	1.6×10^{-9} (950)	5.5×10^{-8} (800)	4.5×10^{-12} (1000)
S_2	8.5×10^{-4} (650)	6.7×10^{-6} (720)	8.1×10^{-6} (800)	8.1×10^{-7} (1000)

In the S-containing atmosphere, when the partial pressure of sulfur in the gas is higher than the value of the metal/metal sulfide equilibrium pressure, then the sulfide may nucleate at the oxide/metal interface. However, the presence of sulfides is not always observed [68-70].

CHAPTER 4

Experiments

4.1 Materials

The scope of the present work is to understand the mechanisms behind the oxidation and corrosion resistance of materials used for turbine blades in aggressive environments. The materials tested include both polycrystalline and single-crystalline nickel-based alloys. Exposures and investigations of both base materials and materials covered with coating were carried on.

Base materials

The investigated substrate materials were polycrystalline and single crystalline Ni-based superalloys IN792 and SCA425+, respectively. The compositions of the materials are listed in Table 3.

Table 3 Nominal composition of the alloys investigated (atomic%)

Alloy	Fe	Cr	Ni	Mo	W	Co	Ta	Ti	Si	Al	C	Other
IN792	0.06	13.9	Bal.	1.10	1.30	8.82	1.32	4.88	0.04	7.36	0.39	Zr, B
SCA425+	0.16	17.1	Bal.	0.62	1.29	4.94	2.63	0	0.04	10.02	0.06	0.03Hf

NiAl- coatings

The coatings applied to the superalloy IN792 were SIF Pt-free or Pt-rich coatings (fabricated by SIFCO Ireland). The SIF Pt-rich coating was produced by electro-plating a 6-8 μm thick Pt layer on a clean alloy surface with a subsequent diffusion heat treatment and a CVD aluminization process. The SIF Pt-free coating was produced in a similar process, but without Pt plating.

4.2 Exposures

Exposures in the simulated environment of industrial gas turbines

Exposures in different gas environments have been carried out: 1. Isothermal oxidation and Na_2SO_4 induced corrosion at 900°C were performed on the material with SIF Pt-free and Pt-rich coatings; 2. Cyclic exposures of the base materials – IN792 and SCA425+, were carried out in 4 different gases, namely $SO_2 + O_2 + H_2O$, $H_2O + O_2$, $SO_2 + O_2 + Ar$ and laboratory air, at 900°C. The cyclic exposures were performed with 65h/cycle, up to 4 cycles.

Exposures of coated samples: IN792 with SIF Pt-free and Pt-rich coatings

A horizontal tube furnace with a quartz tube and an alumina tube was used in the isothermal oxidation and Na_2SO_4 induced corrosion experiments respectively. The oxidation exposures were performed in synthetic air (4:1 N_2 and O_2) with a flow rate of 200 ml/min at 900 °C for 100, 500 and 1000 hours. The Na_2SO_4 induced corrosion exposure was performed in order to simulate continuous contaminant-induced hot corrosion occurring in gas turbines. In this test, the holders for specimens and salt were made of alumina, and the Na_2SO_4 salt container was placed in a zone where the temperature was above 884 °C to provide salt vapor. At the same time, the synthetic air was used as a carrier gas with a flow rate of 200 ml/min. Meanwhile, the samples were put in the

temperature zone above 900 °C to avoid salt condensation on the samples. The corrosion exposures were also performed for 100, 500 and 1000 hours.

Exposures of base materials: IN792 and SCA425+

Cyclic exposures were performed in a tube-type furnace produced by Xerion. The holders for the specimens were made of Kanthal Al, which was preoxidized to form an inert surface layer of α-Al_2O_3, see Fig. 8. A gas flow of 150 ml/min was used in these exposures. The specimens were heated up to 900°C at a rate of 30°C/min, and then kept for 65 hours at that temperature. After that, the samples were cooled down at a rate of 30 °C/min down to 650°C. In case the exposure gas contained H_2O, then the supply of H_2O was turned off to avoid condensation at temperatures below 650 °C. The exposures were performed for 260 hours in the way of four 65-hour cycles. The corrosion experiments were made using the following gas mixtures:

a) SO_2 (3000ppm) + O_2 (69 vol.%) + H_2O (31 vol.%)
b) H_2O (31 vol.%) + O_2 (69 vol.%)
c) SO_2 (3000ppm) + O_2 (69 vol.%) + Ar (in balance)

while the oxidation test used ambient air as the flow gas.

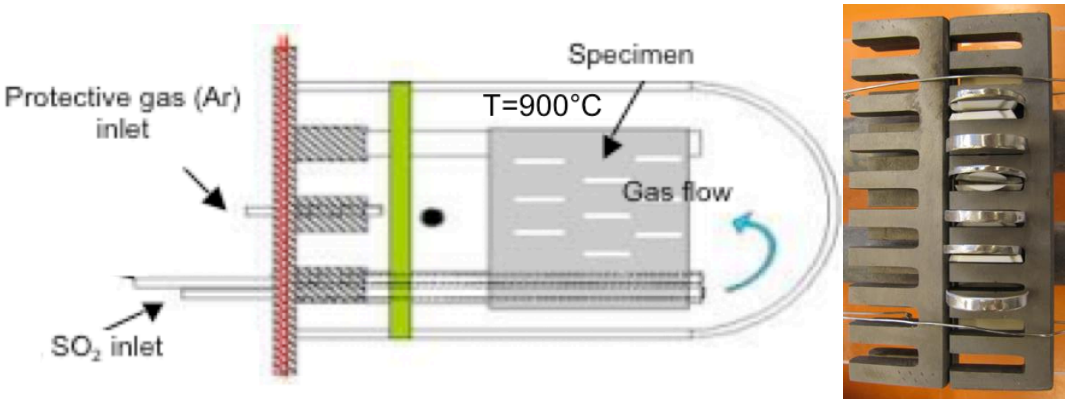

Fig. 8 Schematic image of experimental set-up and a photo of samples and sample holder.

Desulfurization

In order to investigate the influence of S in the alloy on its corrosion properties, samples of SCA425+ were desulfurized using hydrogen annealing as in Fig. 9. The samples were placed in small ceramic boats and inserted in an alumina tube furnace at 1200°C for 100 h. The gas used for desulfurization was 5%H_2+Ar, and its flow rate was 200 ml/min. After the hydrogen annealing, an aging heat treatment at 1100°C for 4 h followed by 20 h at 850°C was used to restore the alloy structure. The same treatment but in pure Ar gas was performed on another set of samples.

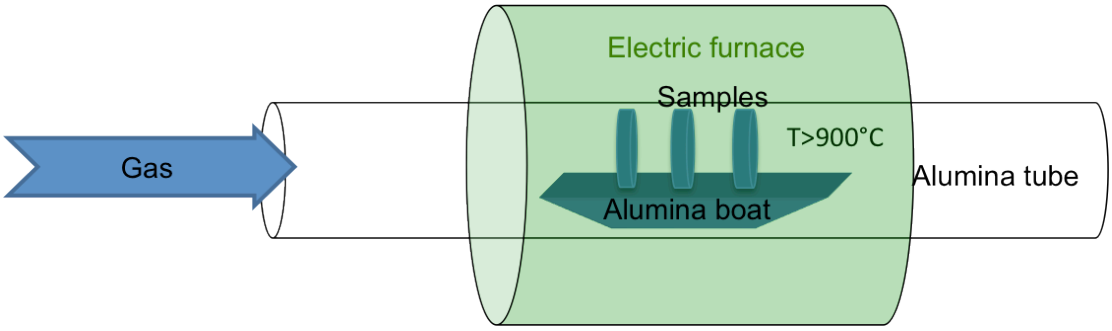

Fig. 9 Schematic image of the hydrogen annealing experiment.

Both sets of samples were then exposed to laboratory air at 1000 °C for 90 cycles using 1 h/cycle.

4.3 Analysis techniques

The materials were analyzed using several different characterization techniques in order to obtain information about the formed oxide structures, chemical compositions and existing phases, and further to understand the oxidation and corrosion mechanisms. In this thesis work, Grazing incident X-ray diffraction was used to identify the oxide phases; Focused ion beam microscopy combined with SEM was used to prepare cross-sections and TEM thin foils; Electron microscopy techniques, like scanning and transmission electron microscopy, in combination with energy dispersive X-ray spectrometry were applied to investigate the oxide morphologies and chemical compositions. Electron backscattered diffraction was also employed to identify the oxide phases.

4.3.1 X-ray diffraction (XRD)

XRD gives information about which compounds and crystalline phases that are present in the material. In this work, a Siemens D5000 powder diffractometer equipped with a Göbel mirror was used to identify the oxide phases. The analyses were made in grazing incidence mode, with lower angle for the thin oxide samples and higher incident angle for the thicker oxide samples. Characteristic Cu Kα radiation (λ= 1.54178 Å) from a copper anode X-ray tube was chosen as the source of radiation.

The X-rays hit the sample surface at an incident angle θ and the radiation is diffracted at an angle θ from the atomic crystal planes (hkl), by satisfying the Bragg equation: $2d_{hkl} \sin\theta = n\lambda$ (n=1, 2, 3…), where d_{hkl} is the inter-planar spacing, λ is the wavelength of the radiation and n is an integer giving the order of diffraction [71]. In general, a low incident angle in the range of 0.3° to 1° is used for samples with a thin oxide, whereas thicker oxide layers need a higher incident angle, like 5° to 10°. Thus, by retrieving the diffraction angle and the intensity of the diffracted beams, the crystal structure and the phase composition can be obtained. As shown in Fig. 10, the X-ray diffractogram can be used to identify the phases appearing in a corroded sample.

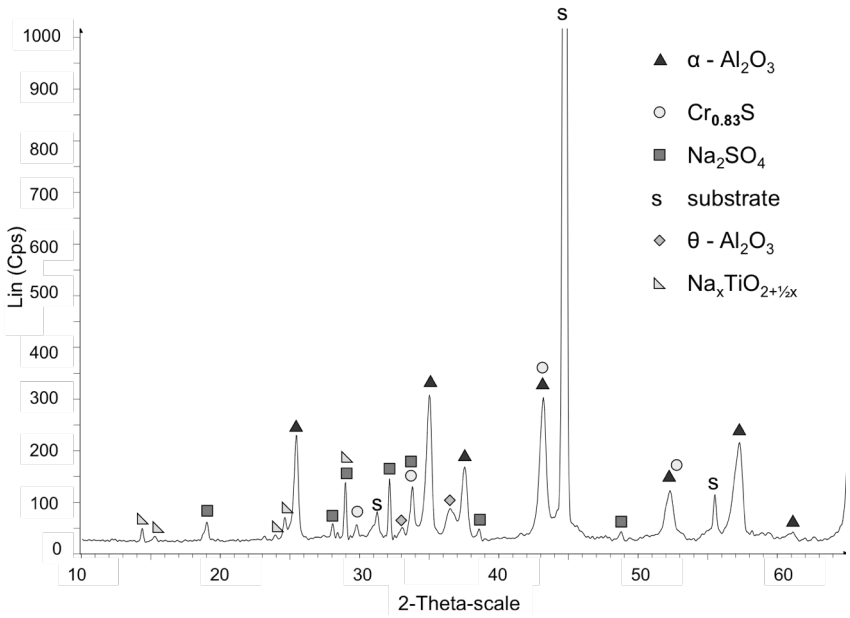

Fig. 10 Diffractogram of IN792 with NiAl coating after being exposed to Na_2SO_4 for 100 hours.

4.3.2 Scanning electron microscopy (SEM)

When a focused electron beam scans across a specimen surface it creates a number of different types of signals, see Fig. 11. The signals commonly used to make SEM images are backscattered electrons and secondary electrons. The detected signal is amplified and transferred to the intensity of the corresponding pixel in the image. After that, the electron beam continues to move to the next position on the sample to generate the image on the computer screen. The scan rate can be high enough to give a "live" image. In order to make a high quality image, though, a slower scan is used.

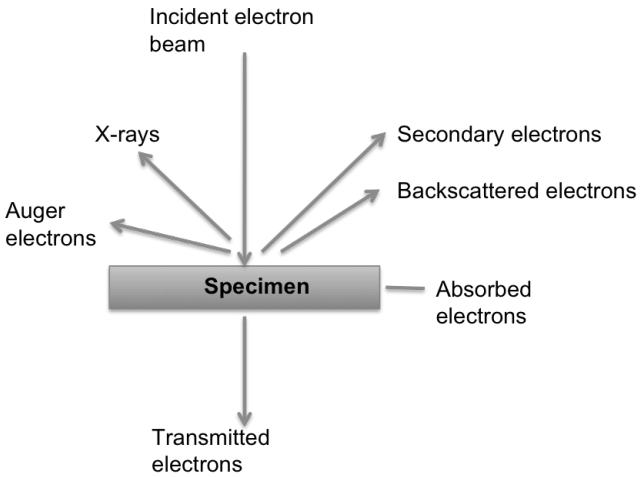

Fig. 11 Some useful signals generated when an electron beam strikes a material.

Image modes

Different operating modes can be chosen to characterize the material, and the choice depends on what kind of feature one wants to investigate and show.

- ***Secondary electrons (SE)***

Normally the secondary electrons are knocked out by the incident beam from a depth smaller than 5 nm from the specimen surface. The energy of the secondary electrons can range from 0 to 50 eV [72]. Because of the small escape depth of SE, this mode gives the highest resolution of surface morphologies.

- ***Backscattered electrons (BSE)***

Backscattered electron energies can range from the primary beam energy E_0 down towards the level of SE energies. The scattering occurs in a volume extending down to about 0.5 μm, depending on the energy of the incoming electrons, below the surface [72]. The higher atomic number elements will give rise to a higher proportion of backscattered electrons. Therefore the contrast in BSE images is given by variations in chemical composition of the sample.

Based on the signals, SEM is generally used to analyze the surface topography and to check the elemental distribution. In this work, FEI Quanta 200FEG-ESEM and Leo Ultra 55 FEG-SEM were used. SEM is applied for imaging top-surfaces and cross-sections. As shown in Fig. 12, SEM secondary images can very clearly show the morphology of the oxides on the surface and in the cross-section, while the backscattered electron images very well show the distribution of elements with different atomic numbers.

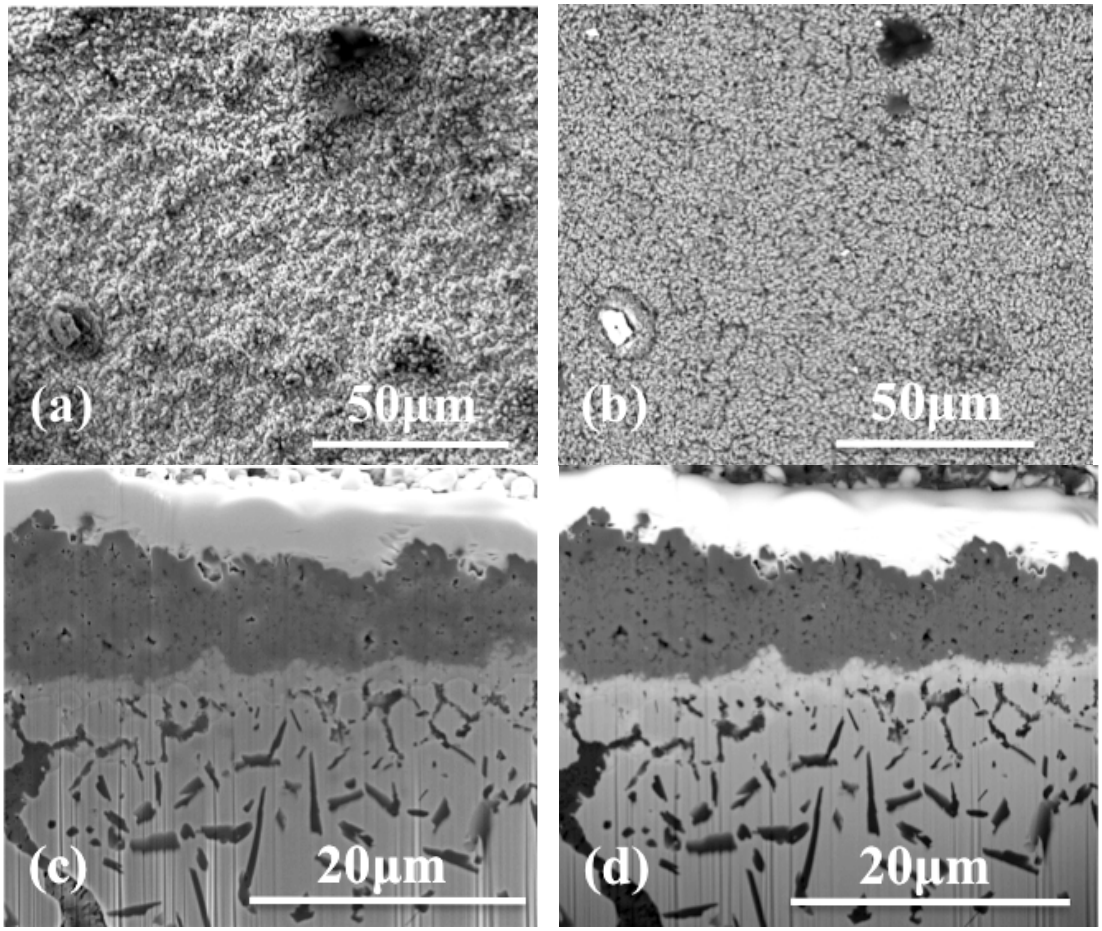

Fig. 12 SEM secondary electron and backscattered electron images of (a)(b) top-view and (c)(d) cross-sections on IN792 exposed to an SO_2 containing mixed gas for 4 cycles of 65 h/cycle.

4.3.3 Focused ion beam (FIB)

A focused ion beam (FIB) microscope operates in a similar way as a SEM. The difference is that FIB uses a finely focused ion beam, with positively charged gallium ions as the primary source. FIB can be used for both ion imaging and as a high precision milling tool. A FIB can also be used to locally deposit Pt (and other metals) from a gas injector. The most impressing feature of FIB imaging is the enhanced crystallographic contrast [73]. As shown in Fig. 13, different grains can be seen on a cross-section thanks to differences in crystallographic orientation.

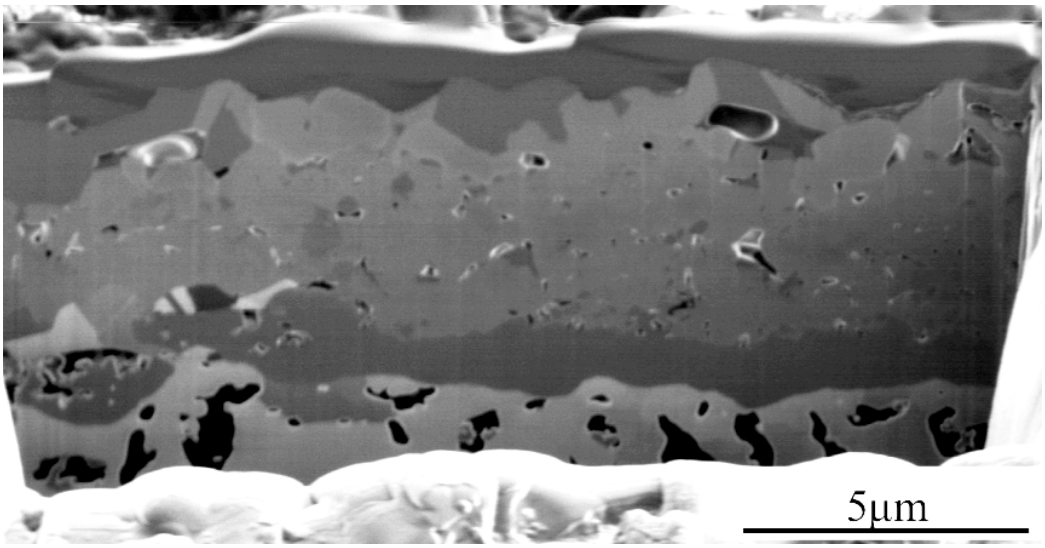

Fig. 13 A FIB image showing strong crystallographic contrast on an ion polished cross-section of IN792 after cyclic exposure to laboratory air for 260 h.

However, because ions damage the specimen much more than electrons, a FIB is often combined with a SEM in the same instrument, a so-called FIB/SEM workstation. In this way, the FIB mode is used for milling and the SEM mode is used for imaging and monitoring of the milling process. Pt-deposition can be made using either ions or electrons. The last method is especially suited for sensitive surfaces. In the present work, a dual-beam FEI Strata 235 FIB/SEM and FEI Versa 3D FIB/SEM were used to make cross-sections for SEM/EDX and the lift-out technique was used to create thin foils for TEM.

Sample preparation of cross-sections for SEM/EDX

In order to check the oxide and the corrosion products beneath the surface by SEM/EDX, cross-sections were prepared using FIB/SEM. To make such cross-sections, a thin Pt-layer is first deposited on the top surface, using electrons, on the feature of interest. This is followed by deposition of a thicker protective Pt-layer using Ga ions. The sample is then tilted 7° and milled along the Pt-strip. As the angle between the ion and the electron columns is 52°, the created cross-section is inclined 45° to the surface. After several milling steps, using decreasing ion currents from 20 nA to 500 pA, gradually, the 45° cross-section is ready for SEM/EDX characterization.

Sample preparation of TEM specimens

The in-situ FIB lift-out technique is used to produce TEM specimens without the need of prior specimen preparation. The lift-out technique is illustrated in Fig. 14.

In the same way as for cross-sections, the interesting area, having a size of 15 µm x 2 µm, is protected by both electron and ion Pt deposition (Fig. 14a). Thereafter, two trenches (25 µm x 12 µm) are created by milling away the material along both sides of the Pt strip. Hereby, the interesting area becomes a foil that still sticks to the bulk material (Fig. 14b). The next step is to mill through the foil to cut the foil free, except for two thin "bridges" connecting to the bulk material close to the top surface (Fig. 14c). Then the so-called omniprobe needle (a sharp tungsten needle that can be moved with high precision) is inserted and approached as close as possible to one side of the Pt strip. Pt is deposited to attach (by soldering) the foil to the omniprobe needle at the contacted area (Fig. 14c). In the next step the foil is cut free from the material by ion milling (Fig. 14d), after that the foil is lifted out and moved to a Cu TEM-grid (Fig. 14e). Then the lifted-out foil is attached to the grid by Pt deposition and milled free from the omniprobe. Finally the lifted-out section (Fig. 14f) is thinned down by ion milling at successively decreasing the current in order to get an around 100nm thick TEM sample.

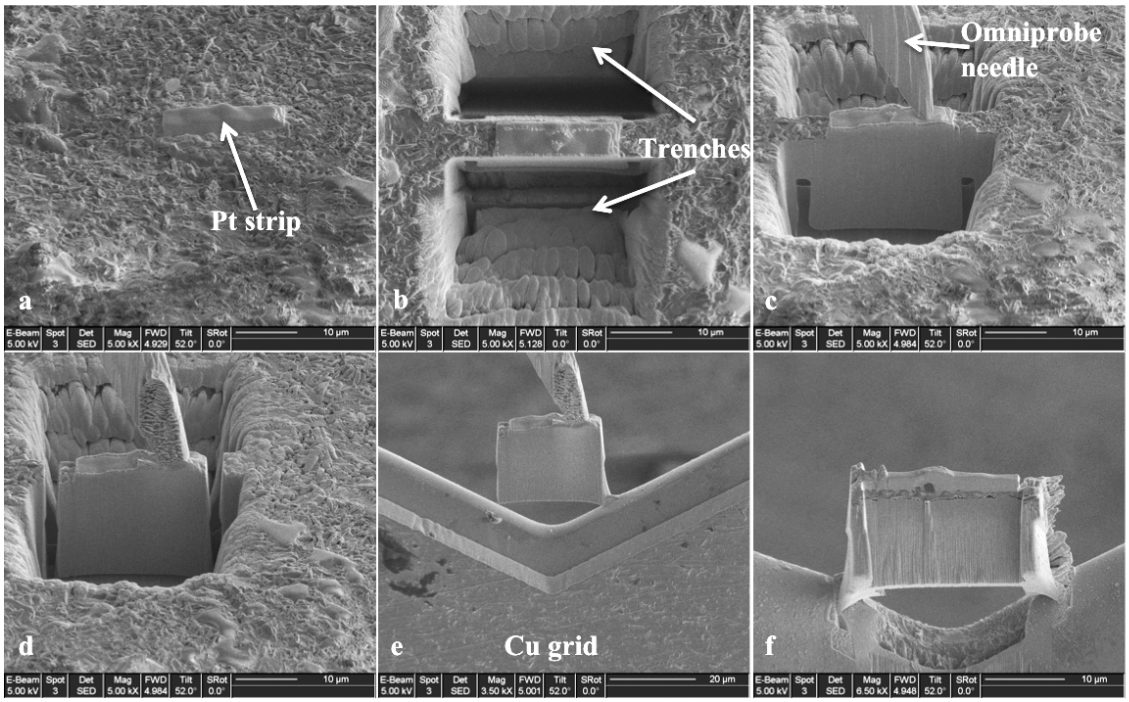

Fig. 14 FIB in-situ lift-out technique (a-f) for TEM samples.

4.3.4 Energy - dispersive X-ray spectroscopy (EDX)

Energy dispersive X-ray spectroscopy (EDX) is a technique to use X-ray spectroscopy to determine the local chemical composition of a material. When the incident electron beam knocks out an inner-shell electron, an electron from an outer electron shell will jump into the inner shell. The difference in energy between the two shells of the atom is emitted as a characteristic X-ray photon. Different elements have different energies of the characteristic X-rays, which can provide a "fingerprint" of the element.

The application of EDX is always combined with SEM or TEM to obtain the qualitative or quantitative elemental composition. It can also be used to visualize

the elemental distribution in the area of interest, so called elemental mapping, see Fig. 15.

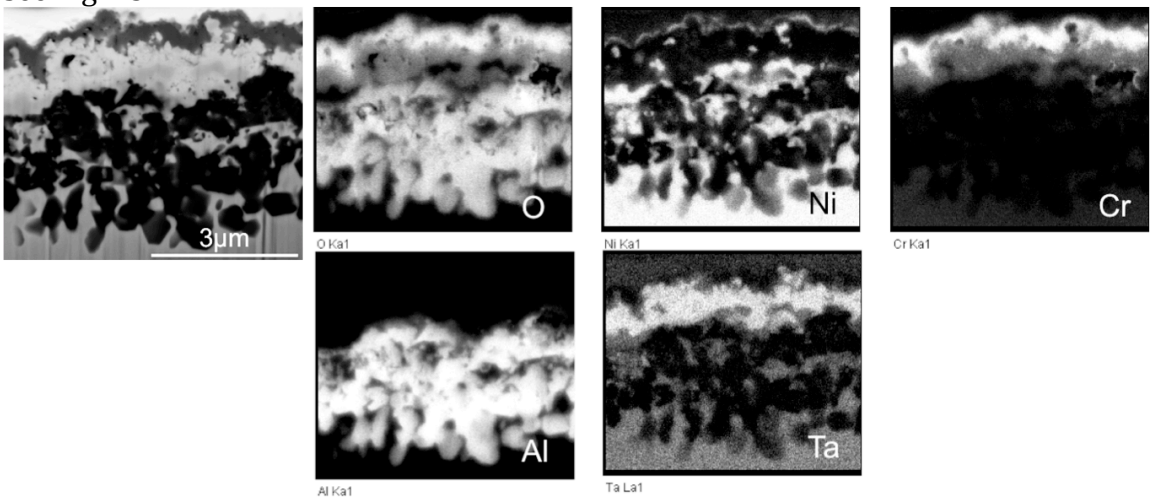

Fig. 15 EDX quantitative maps of different elements on cross-section.

4.3.5 Transmission electron microscopy (TEM)

Transmission electron microscopy combined with EDX is very useful for investigating microstructures and chemical composition with high resolution. Very fine structures that cannot be distinguished by SEM, can often be resolved by TEM. In this work, a FEI Tecnai T20 (operated at 200 kV was used) and a FEI Titan 80-300 (operated at 300 kV) were used.

TEM imaging modes

A TEM image is usually obtained either as a bright filed (BF) image or a dark field (DF) image. By positioning an objective aperture in the back focal plane of the objective lens, either the direct (non-diffracted) electron beam is allowed to pass through, or only one of the diffracted beams is allowed to pass through. In the former case a BF image is formed and in the latter case a DF image is formed, see Fig. 16. In a DF image only areas giving rise to diffraction in the chosen direction appear bright, and thereby crystallographic information can be visualized.

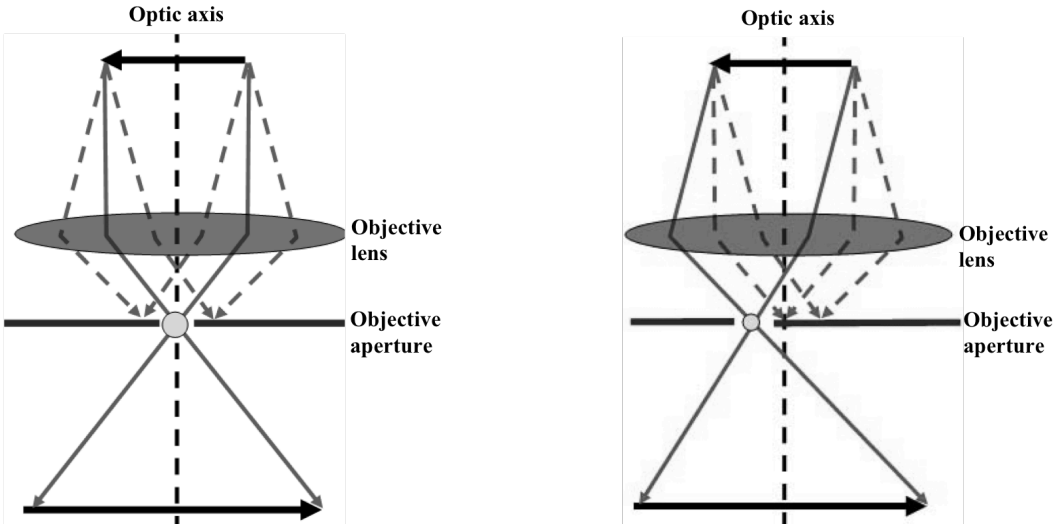

(a) *(b)*

Fig. 16 Schematic description of TEM beam paths for (a) bright field and (b) dark field images [74, 75].

Scanning transmission electron microscopy (STEM)

In scanning transmission electron microscopy, also a direct or a scattered beam is chosen for imaging, but in this case detectors, rather than apertures, select the beams. In STEM, a BF detector or an annular DF detector is used. By controlling which electrons fall on which detector, a DF or BF STEM image will be obtained. When the direct electron beam is collected by the BF detector, the formed image is called a STEM bright field image. When scattered electron beams are collected by the annular DF detector, a STEM dark field image is formed [75]. Typical BF and DF STEM images are shown in Fig. 17.

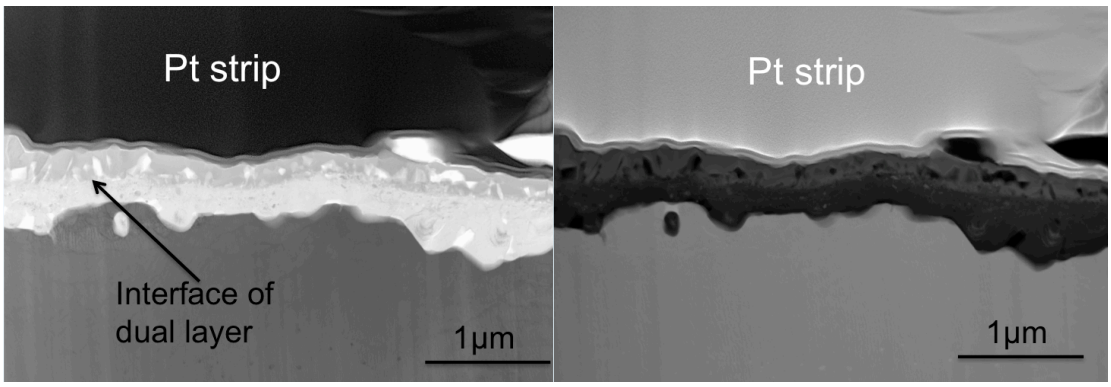

(a) *(b)*

Fig. 17 (a) Bright field and (b) Dark field STEM image of an SCA425+ sample after 4-cycles exposure in laboratory air at 900 °C.

Besides the function of imaging, when the specimen is crystalline, diffraction patterns (DPs) will form at the back focal plane of the objective lens. This will give direct crystallographic information of material.

4.3.6 Electron backscattered diffraction (EBSD)

Electron backscattered diffraction (EBSD) is a microstructural-crystallographic technique to measure the crystallographic orientation in SEM. In general, a stationary electron beam strikes a tilted crystalline sample, and then the diffracted electrons form patterns on a fluorescent screen. The different planes in the material diffract different electrons into so-called Kikuchi bands. If the system geometry is designed well, it is possible to relate the bands present in the pattern to the underlying crystal phase and the orientation of the material within the electron interaction volume. Each band can be indexed individually by the Miller indices of the diffracting plane, which formed it. The resolution of EBSD is related to the resolution of the SEM, for modern field emission SEMs, 10nm grains can be measured [76, 77]. EBSD is a very powerful tool for microstructural characterization, and it is used to measure crystal orientation, grain size, phase identification, etc. [78].

Normally EBSD operates on a flat, highly polished bulk sample at shallow angle to the incident electron beam. A new approach to SEM-based diffraction using an electron transparent sample coupled with conventional EBSD hardware and software has emerged, and was used in the present work. It is called transmission EBSD (t-EBSD) [79]. Fig. 18 represents a SEM transmission Kikuchi diffraction pattern from a TEM film showing the presence of a α-Al_2O_3 phase.

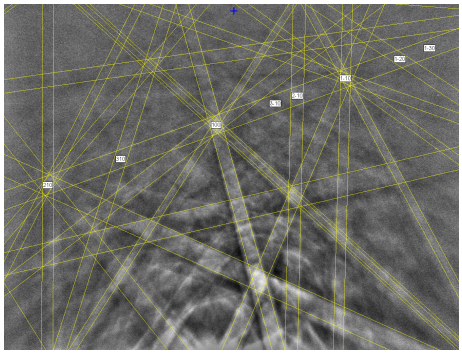

Fig. 18. SEM transmission Kikuchi diffraction (TKD) pattern of α-alumina from TEM thin film at 20 kV.

CHAPTER 5

Results and Discussion

The aim of the present work is to investigate the high temperature oxidation and corrosion of Ni-based superalloys used in the blades of industrial gas turbines. The focus is on the properties of the formed oxides in different working conditions. Advanced microscopy (SEM and TEM) and microanalysis techniques were used as experimental tools.

5.1 The influence of the material on the corrosion behavior

The oxidation and corrosion resistance of alloys operating at elevated temperatures relies on the formation of a compact and continuous protective oxide scale. Besides the environment, there are several other factors such as material composition, surface treatment, etc., which influence the oxidation and corrosion behavior of the alloy.

5.1.1 Surface treatment

The surface treatment, such as grinding, polishing, sandblasting, etc, influences the defect density in the subsurface zone of the material. The generated defects provide fast paths for elemental diffusion. Thus, the surface condition of the material before the exposure plays an important role for the material oxidation and corrosion behavior.

The effect of surface treatment on the corrosion behavior of Ni-base superalloys (the newly developed SCA425+ and the extensively used IN792) was studied in Paper IV. In this work for each material, samples were either ground using 600 grit SiC paper or polished with 3 μm diamond paste. Cyclic exposures were carried out at 900°C. The duration of the cycles used was 65 h and one to four cycles were applied in this study. The investigations show that the SCA425+ alloy is a borderline alumina former at 900°C. It may form a thin and protective alumina layer, provided that it receives surface treatment that creates a zone of defects allowing for a fast enough supply of Al to the metal surface. In such case, a thin and protective Al_2O_3 oxide scale might form. This is demonstrated in Fig. 19a, which shows the oxide formed on a ground sample after 65h exposure at 900°C. However, due to slow supply of Al in the polished SCA425+, Fig. 19b, a layered oxide scale, that includes $NiCr_2O_4$, Cr_2O_3 and $CrTaO_4$, is formed. Below this scale internal oxidation of aluminum takes place. Thus, the investigation reveals an alternative way of improving the corrosion properties of this ally.

On the other hand, the corrosion behavior of IN792 is not as sensitive to the surface treatment. The material is not only unable to form a protective alumina layer, but also it does not form a protective chromia layer since the Cr-rich oxide is small-grained and porous. The introduced dislocations from the surface cold work cause recrystallization of the near surface layer with subsequent corrosion attack at the grain boundaries in the newly formed metal grains, see Figs. 19c and 19d, where the grain size in the ground sample is smaller than in the polished one.

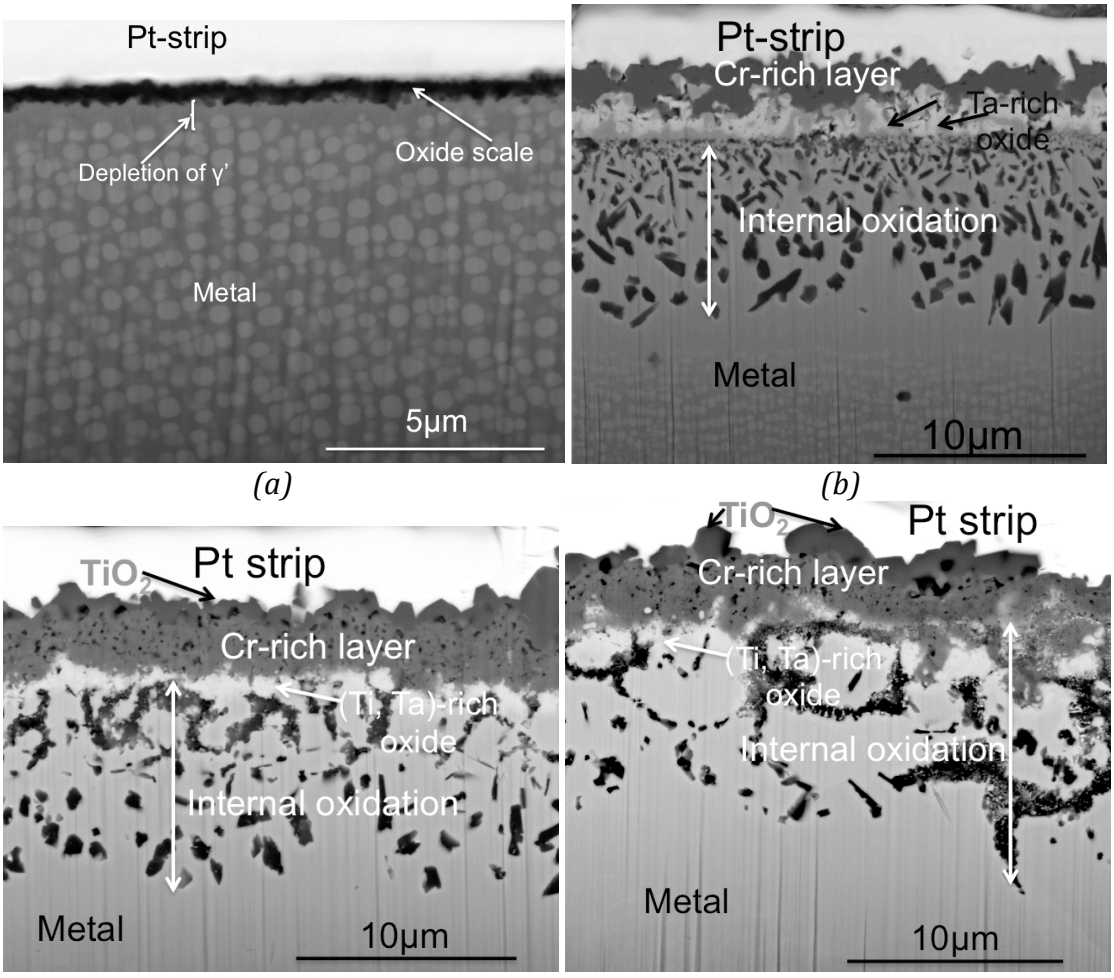

Fig. 19 BSE SEM images of cross-sections of (a) ground and (b) polished of SCA425+; (c) ground and (d) polished IN792 after 65h exposure in SO_2 containing gas.

5.1.2 Influence of alloying elements and impurities

The role of Pt in oxidation and corrosion resistance

The application of protective coatings is one of the most efficient ways to reduce the environmental degradation, and diffusion aluminide coatings have often been used for this purpose in industrial gas turbines. To further improve the protective properties, some alloying elements are usually added to the coatings. One of these elements, known to prolong the life of components is Pt. The effects of Pt on high temperature oxidation resistance of coatings have been presented in numerous studies [30, 80], but the influence of Pt on the corrosion resistance is less well documented [78]. Thus, the effect of Pt on the resistance of the coatings against hot corrosion was investigated in this work, Paper I. In order to simulate continuous contaminant-induced hot corrosion occurring in gas turbines, a new method in which Na_2SO_4 salt was evaporated in the furnace was developed, Paper III. This method is less time- and operator-demanding than methods based on ex-situ salt spraying and is therefore suitable for long-time exposures.

To prevent salt condensation on the samples, the salt boat was placed in a region where the temperature was above 884°C, while the specimens were kept at 900°C. Synthetic air (4:1 N_2 and O_2) with the flow rate of 200 ml/min was used as carrier gas. Exposures were performed both in synthetic air and in gas containing Na_2SO_4 salt vapor at 900°C for 100 h to 500 h.

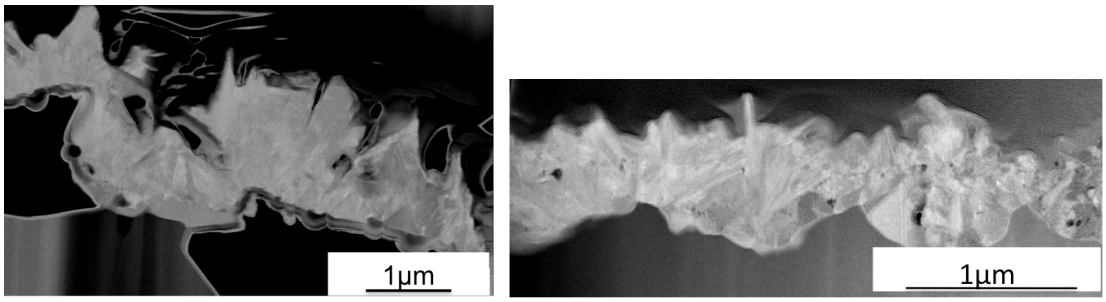

(a) *(b)*

Fig. 20 Dark field STEM images of TEM thin foils of (a) Pt-free and (b) Pt-rich coatings after 100h oxidation in synthetic air at 900°C.

It has been shown that many voids appear at the oxide/metal interface after 100 h oxidation in air of the Pt-free coating. The presence of Pt in the coating prevents the formation of voids, see Figs. 20a and 20b. It was proposed that Pt suppresses the formation of cavities by facilitating faster diffusion of Al ions, which can fill the voids.

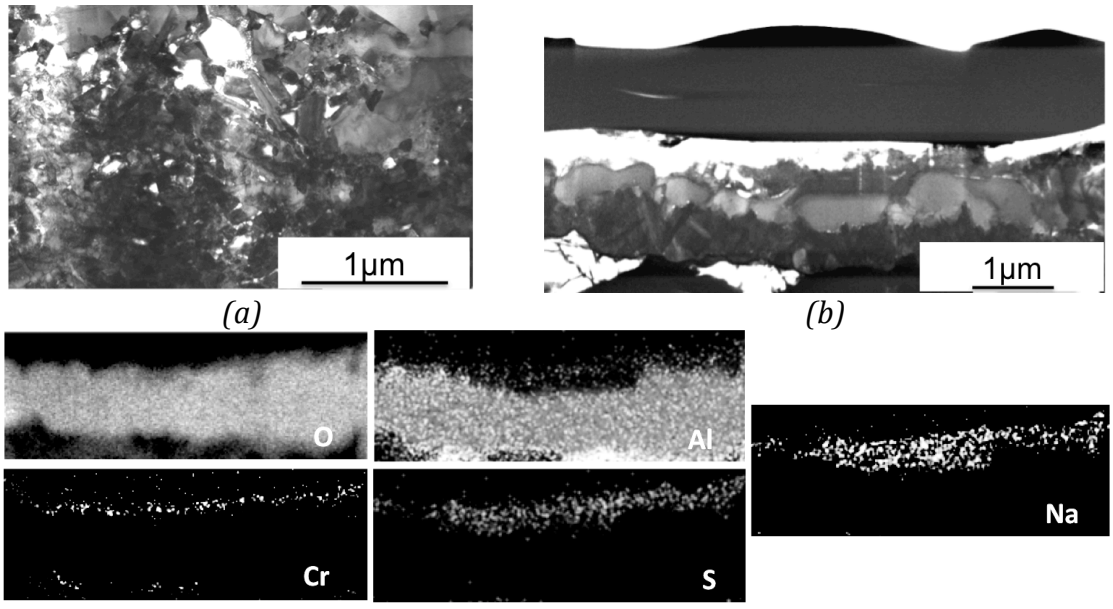

(a) *(b)*

(c)

Fig. 21 Microstructure of the oxide scale on (a) the Pt-free coating and (b) the Pt-rich coating after 100h corrosion in Na_2SO_4 gas at 900°C; (c) Corresponding quantitative EDX maps of O, Al, Cr, S and Na on the TEM thin foil in (b).

Exposures to Na_2SO_4 vapor have been proved to create much faster-growing oxides on Pt-free coatings. As shown in Fig. 21a, after 100 h of exposure, the formed oxide scale in a Pt-free coating is fine-grained and contains many pores and cracks. Also areas rich in S, Na, Cr and Ti were observed at the oxide/metal

interface, indicating that the propagation stage of corrosion had already started. On the other hand, the oxide scale formed on the Pt-rich NiAl coating was thinner and denser, as shown in Figs. 21b and 21c. Thus, the Pt-rich coating is proved to be protective even after 500 h exposure, but the observed voids at the oxide/metal interface indicated limited adherence of this oxide.

Influence of S content on the oxidation behavior (not published)

An attempt to study the influence of S on the oxidation behavior of the newly developed alloy, SCA425+, was undertaken. The original S content in the material was relatively high, 17 ppm. Desulfurization was performed using hydrogen annealing. However, it turned out that this treatment was not completely successful since the content of S decreased only to 12 ppm. This was most possibly due to the formation of a thin oxide layer during desulfurization that prevented effective removal of S. Nevertheless, studies of desulfurized and original samples subjected to cyclic (1h/cycle) exposures in laboratory air at 1100°C show that spallation on the sample containing higher S is more pronounced, see Fig. 22. Thus, as expected, S degrades the adherence of the oxide scale.

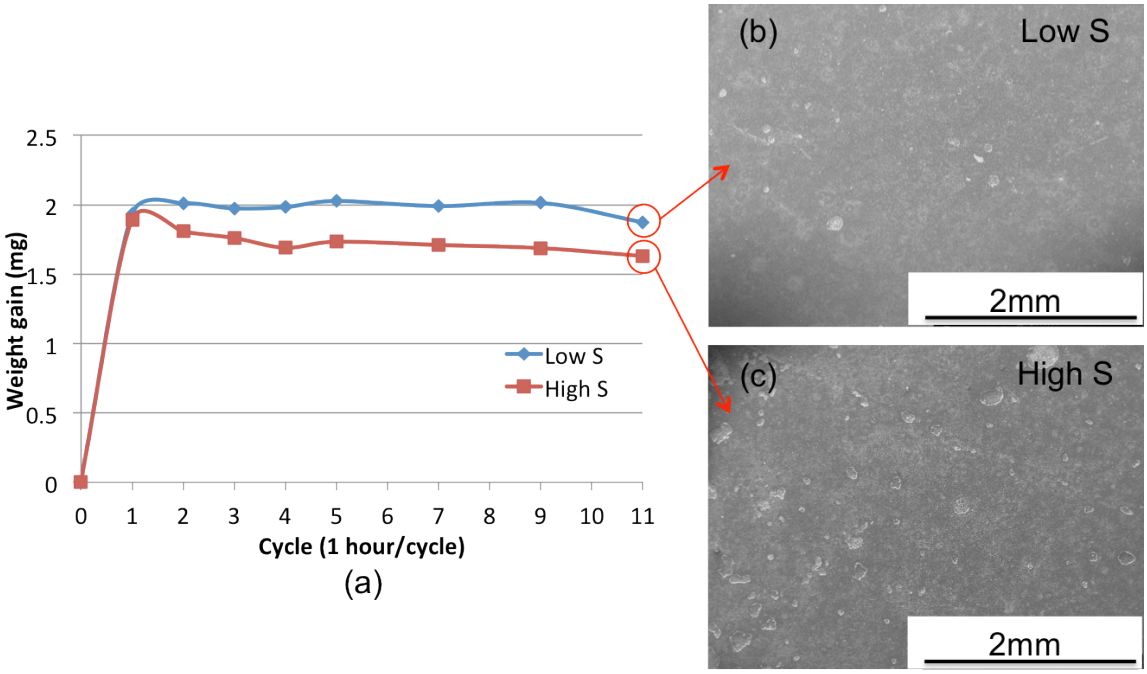

Fig. 22 (a) weight gain of SCA425+ samples containing low S and high S and SEM top view images of SCA425+ sample containing (b) low S and (c) high S after 11 cycle exposures at 1100°C.

Influence of the amount of Cr and Al in the alloy

In this work the difference in the corrosion behavior of two nickel-based superalloys, IN792 (14Cr-7Al-5Ti-1Ta-Ni bal. in at.%) and SCA425+ (17Cr-10Al-3Ta-Ni bal.) was studied (Paper II, IV and V). SCA425+ was recently developed for future use in IGT for electricity generation. Its Cr content, 17 at.%, is substantially higher than for the existing single-crystal superalloys, and it also contains a relatively high amount of Al, 10 at.%. The mechanical testing of the new alloy shows that its thermo-mechanical fatigue performance is superior to the alloy IN792, which is commonly used for similar applications, and

comparable to that of the older single-crystalline superalloy CMSX-4. The present investigation shows that the SCA425+ material is able to form a protective continuous alumina layer given suitable surface treatment. On the other hand, the IN792 material does not form a protective oxide scale in any of the investigated conditions and the structure and morphology of the oxide scale are not very sensitive to the surface treatment.

5.2 The influence of the environment on the corrosion behavior

It is well recognized that corrosion attacks depends on the environment to which the material is exposed. Much research has focused on high temperature corrosion of metals in the presence of salt and SO_2 [36, 65, 81-83]. One of the objectives of this work was to investigate the corrosion resistance of the newly developed nickel-based alloy SCA425+ in different surroundings and to compare the results with those for the extensively used IN792, see Fig. 23 (Papers II, IV and V).

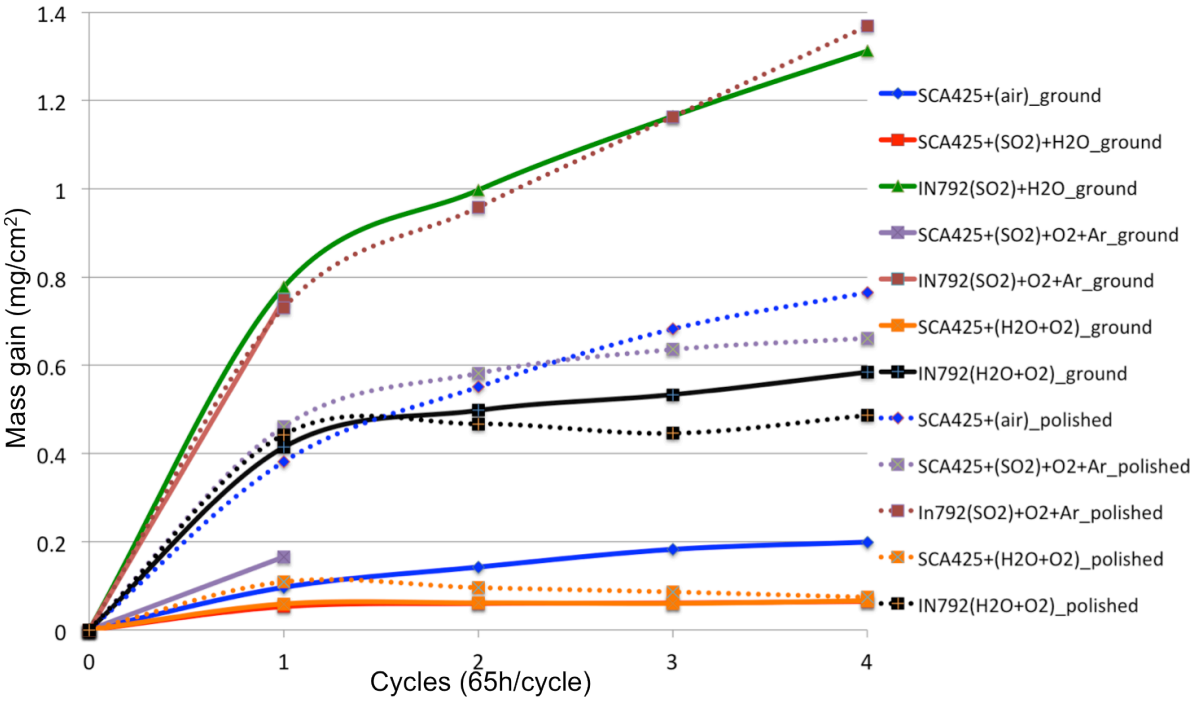

Fig. 23 Mass gain of SCA425+ and IN792 samples under different surface treatment and exposure conditions (Dashed lines belong to the polished samples and solid lines belong to the ground samples).

5.2.1 Influence of water vapor

It is generally accepted that water vapor has a major effect on the oxidation rate of chromia-forming iron-based alloys (steels) and often increases the oxidation rate by an order of magnitude. This is in many cases attributed to the failure of the protective Cr_2O_3 layer by the formation of the volatile $CrO_2(OH)_2$ [52, 84, 85]. It is also debated that the water vapor might affect the selective oxidation of aluminum and chromium in Fe-based alloys [43]. The oxidation behavior of high-temperature Ni-based alloys in steam has received relatively little attention and the effect of water vapor on these types of alloys is not so clear, due to contradictory results [86].

The investigation performed during this work reveals different corrosion behavior when the single-crystalline material SCA425+ in a polished condition is exposed to laboratory air (containing only 1 vol.% H_2O) or to the 69 vol.%O_2 + 31 vol.%H_2O environment at 900°C see Figs. 23 and 24**.** In the dry condition the evaporation of Cr is not obvious. In the presence of moisture the Cr-rich oxide layer is thinner due to vaporization of Cr through the formation of $CrO_2(OH)_2$ and big blade-like Cr_2O_3 oxide particles exist on the sample surface. To estimate the loss of chromia a comparison of the Cr depletion in the metal with the amount of Cr_2O_3 was used. The results also indicate that the volatilization of chromia slows down with increased exposure.

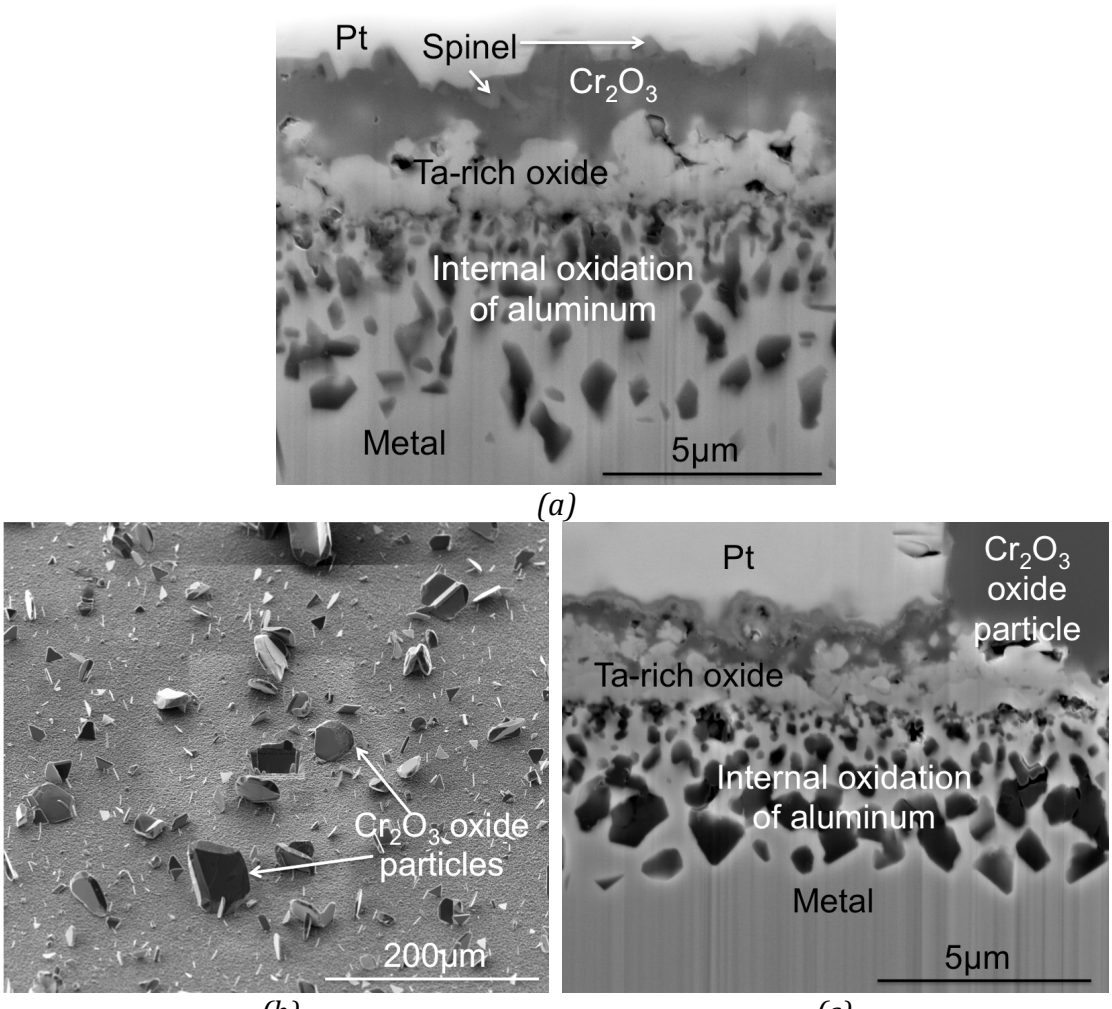

Fig. 24 SEM images of SCA425+ (a) exposed to laboratory air, (b) the top surface and (c) the cross-section of SCA425+ exposed to the humid environment (containing 31 vol.% H_2O) at 900°C for 65h.

5.2.2 Influence of SO_2 gas

One of the important questions to answer was if and how the presence of SO_2 in the environment was influencing the formation and possible spallation of the oxide scale. The last mentioned property is of special importance for the applications in which the alloys are coated by a thermal barrier coating. The lifetime of coated components largely depends on the adherence of the formed oxide scale. The long-term goal is to be able to accept more flexible fuel

specifications for natural gas that contains significant concentrations of H_2S.

As shown in Figs. 25a and 25b, the morphology and layered structure of the oxide scale on SCA425+ samples exposed to laboratory air and gas containing 3000 ppm SO_2 (Paper II and IV) are very similar. The main difference is that a quasi-continuous alumina layer forms at the front of the internal oxidation when SO_2 is present in the gas. The result is very consistent with recent studies [68], that have shown that the addition of small amounts of SO_2 in the atmosphere can promote the transition from internal to external alumina scales. It should also be mentioned, in this context, that the effect of moisture in the work presented in Paper II was underestimated.

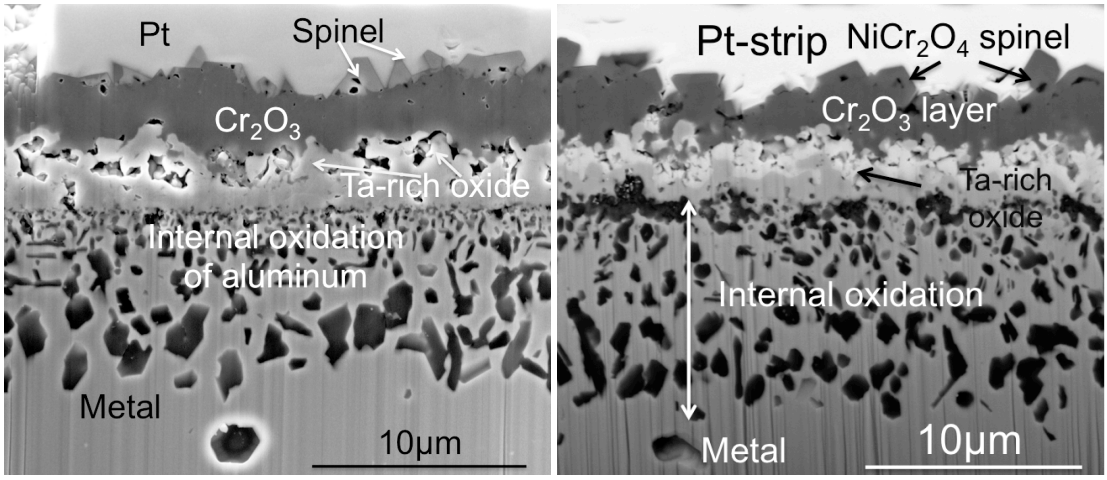

(a) *(b)*

Fig. 25 Back scattered electron (BSE) SEM cross-section images of SCA425+ samples exposed to (a) laboratory air and (b) SO_2 containing gas for 260h.

5.2.3 Influence of sulfates

The industrial gas turbine working environment is rather complex, and hot corrosion often takes places in the presence of various salts, e. g. Na_2SO_4. Thus, the oxidation resistance of coatings on IN792 alloy in air and Na_2SO_4-containing gas was compared (Paper I and II). It has been shown that the exposure to Na_2SO_4 salt vapor produces a thick and small-grained scale on the Pt-free coating already after 100 h of exposure, while the scale is compact and uniform in the case of exposure in air, see Figs. 26a and 26b. After prolonged exposure in the salt vapor the low Al content (about 29 at.%) close to the coating surface proves that the coating loses its protectiveness.

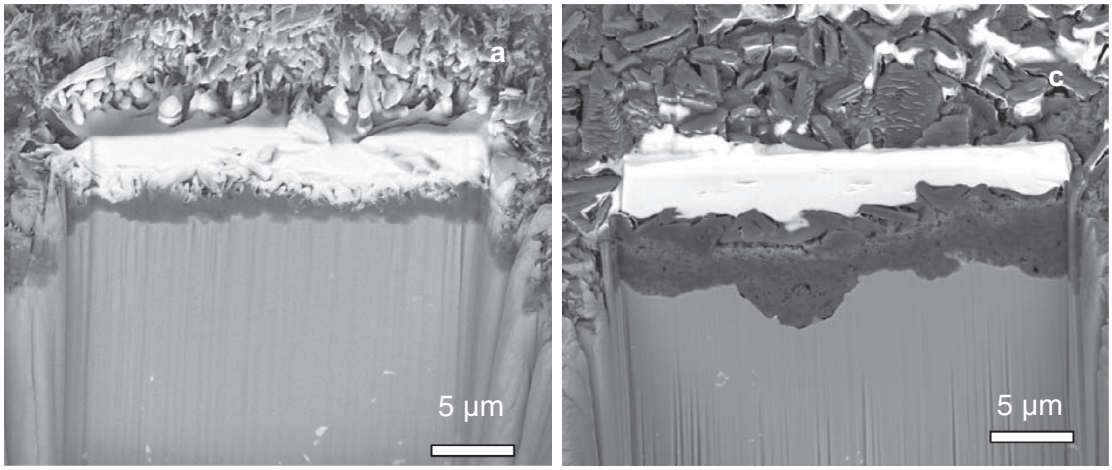

(a) *(b)*

Fig. 26 Cross-section SEM micrograph of samples of SIF232 aluminide coatings after (a) oxidation in synthetic air and (b) the Na_2SO_4 gas.

Furthermore, the formation of sulfides at the oxide/metal interface was observed, Fig. 27. It is suggested that the sulfides have to form either by the reaction with Na_2SO_4, which has penetrated through cracks in the scale, or by the reaction with SO_2 from the atmosphere.

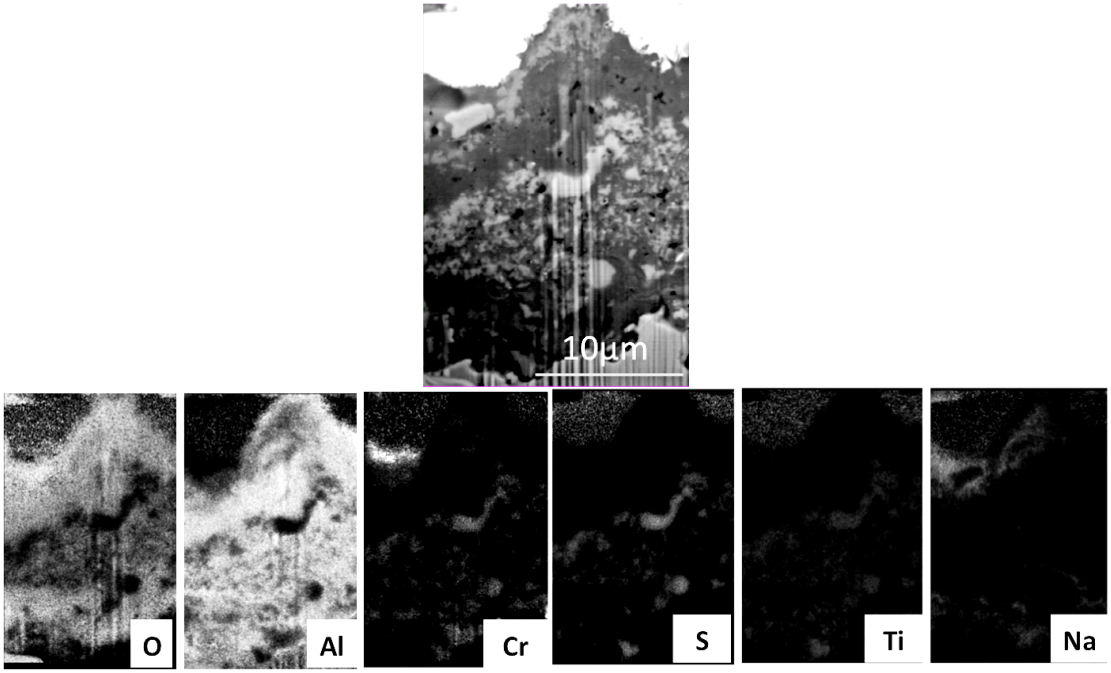

Fig. 27 SEM cross-section image of the sample with Pt-free coating and corresponding quantitative EDX maps of O, Al, Cr, S, Ti and Na on the cross-section, after 500h corrosion in the in-situ corrosion exposure with $NaSO_4$ gas at 900°C.

5.3 Future work

It would be interesting to do further investigation of

1. The influence of surface treatment.
   More detailed studies including both different temperatures and exposure times should be performed. That will provide a quantitative

understanding of changes in the diffusion process and will allow for optimization of the surface treatment.

2. The investigation of the effect of S in the material on the corrosion resistance should be continued. Desulfurization process of SCA425+ should be repeated to obtain material with very low S content. Considering the practical working time of turbine blades, longer exposures are also proposed.

3. The effect of SO_2 on corrosion behavior
   Shorter and longer exposures are suggested, because it will help to understand whether the sulfate forms at the early stage and then stops further sulfurizing of the oxides or if it is just because the exposure time is not long enough to form the sulfides in the scales. It was reported that the Cr-volatilization is restricted by the presence of sulfur [87], so the exposures with short time, like 1 h, in SO_2 + H_2O is recommended.

4. The effect of H_2O
   Performing exposures of IN792 and SCA425+ in H_2O and O_2 for much shorter times, like 10 min., 1h, 24h is also necessary. This would help to understand how the big Cr_2O_3 particles form on the specimen surface. It is also suggested to perform the exposures in 69 vol.%O_2 with Ar in balance, so that the possible influence of 1 vol.% H_2O from air can be avoided.

Acknowledgement

There are many people who have contributed to this work. Here I would like to express my appreciation to the people involved in my work, the ones provided selfless help during these years and the ones who encouraged me all the way in both my job and life:

Here I would like to sincerely express my appreciation to my supervisor - Prof. Krystyna Stiller for giving me the chance to start my research life as a project assistant since 2009 and then continue my Phd study. I am very grateful for her patient guidance and warm encouragement all the time not only in my work but also to my life! Thanks for spending your time for discussions and all the effort on giving helpful comments on my articles and thesis! A lot of thanks to you for being open-minded to me when we had different opinions!!

I want to thank Prof. Lars-Gunnar Johansson for helpful advices, sharing your knowledge in the corrosion field, spending your time on my project meetings, giving suggestions for the experiments when I performed the exposures in the Environmental Inorganic Chemistry group, discussing and resolving the problems during my articles' writing. I am benefited from all your help and would like to express my deep appreciation to you!

I would like to thank my co-supervisor Dr. Mattias Thuvander for supporting and inspiring me during the research work and spending time on my articles and thesis work.

My thanks go to Fredrik Karlsson, Helena Oskarsson, Xinhai Li, Rikard Norling, Peter Viklund, Kenneth Göransson, Jiaxin Chen, Charlotta Gustafsson and Yu Cao for the project collaboration.

My thanks also go to Prof. Mats Halvarsson for guiding me in the world of microscopy, and very helpful suggestions on the analysis of my microscopy work.

Many thanks to Dr. Anders Kvist for the instrumental support and patiently answering my questions on the techniques; Ola Löfgren for always giving me computer support; Helen Lejon for great help and Josephine Green for the administrative help.

I also appreciated to the help I got from the people in HTC. Because of you, my work became much easier!

I would like to thank all the senior scientists and former and present Ph.D students in the group of Materials Microstructure and Eva Olsson's Group. I am very happy for the enjoyable working environment you all have created! Thanks for bringing the funny jokes and "intelligent and brilliant information" to delight me; thanks for the wise suggestions and encouragement when I got lost; thanks for sharing with me a lot of 'the first time' experience – swimming, skating, yoga… thanks for selfless help, encouragement and support for everything; thanks for the nice conversation, cappuccino time and enjoyable summer lunch

time in our “secret place”; thanks for the ‘exhausted’ hiking and wonderful experience in France!.....A lot of thanks to you all surrounding me and the moments you shared with me……..! Finally thanks everyone here in the groups, you never know how much I appreciate to work with you here!

Finally but not the least, I would like to thank my loving family – without your support, I could not manage to finish my work and I could not be stronger, braver and happier! 我最后最深沉的爱献给我最心爱的女儿姚舒雯，工作对我来说很重要，但只是一小部分，而你却是我生命中很重要的部分。看着你健康快乐的成长，我所做的一切都是值得的！

References

1. http://www.mpoweruk.com/energy_resources.htm.
2. http://en.wikipedia.org/wiki/Fossil-fuel_power_station.
3. http://www.mpoweruk.com/fossil_fuels.htm.
4. http://www.wartsila.com/en/gas-turbine-for-power-generation.
5. R. C. Reed, The superalloys Fundamentals and Applications, Cambridge University, U. K., 2006.
6. G. R. Krishna, et al., *Role of Pt content in the microstructural development and oxidation performance of Pt-aluminide coatings produced using a high-activity aluminizing process.* Materials Science and Engineering: A, 1998. **251**(1-2): p. 40-47.
7. H. Svensson, M. Christensen, P. Knutsson, G. Wahnström and K. stiller, *Influence of Pt on the metal/oxide interface during high temperature oxidation of NiAl bulk materials.* Corrosion Science, 2009. **51**(3): p. 539-546.
8. Y. Zhang, et al., *Effects of Pt Incorporation on the Isothermal Oxidation Behavior of Chemical Vapor Deposition Aluminide Coatings.* Metallurgical and Materials Transactions A, 2001. **32**(7): p. 1727-1741.
9. A. L. Purvis and B. M. Warnes, *The effects of platinum concentration on the oxidation resistance of superalloys coated with single-phase platinum aluminide.* Surface and Coatings Technology, 2001. **146-147**(0): p. 1-6.
10. J. Smialek, *Adherent Al_2O_3 scales formed on undoped nicrai alloys.* Metallurgical Transactions A, 1987. **18**(1): p. 164-167.
11. G. H. Meier, F. S. Pettit and J. L. Smialek, *The effects of reactive element additions and sulfur removal on the adherence of alumina to Ni- and Fe-base alloys.* Materials and Corrosion, 1995. **46**(4): p. 232-240.
12. J. Bressers, S. Peteves and M. Steen, *Coatings for hot section gas turbine components*, in *European Structural Integrity Society*, Elsevier, 2000. **26** p. 115-134.
13. G. Y. Lai, High Temperature Corrosion and Materials Applications, ASM international Science Park, USA, 2007.
14. N. J. Simms, A. Encinas-Oropesa and J. R. Nicholls, *Hot corrosion of coated and uncoated single crystal gas turbine materials.* Materials and Corrosion, 2008. **59**(6): p. 476-483.
15. Y. Tamarin, Protective Coatings for Turbine Blades, ASM International Materials Park, USA, 2002.
16. R. C. Reed, J. J. Moverare, A. Sato, M. Hasselqvist and F. Karlsson, *A new single crystal superalloy for power generation applications.* Superalloys: 12th International Symposium on Superalloys, 2012.
17. S. Bose, High Temperature Coatings, Elsevier Inc, Oxford, 2007.
18. M. Konter and M. Thumann, *Materials and manufacturing of advanced industrial gas turbine components.* Journal of Materials Processing Technology, 2001. **117**(3): p. 386-390.
19. R. Sivakumar and B. L. Mordike, *High temperature coatings for gas turbine blades: A review.* Surface and Coatings Technology, 1989. **37**(2): p. 139-160.
20. C. SIM, N. Stoloff and W. Hagel, Superalloys II, John Wiley & Sons, New York, 1987.

21. M. Åsa, *Ageing Influence on Nickel-based Superalloys at Intermediate Temperatures (400–600°C).* Master Theis, Luleå University of Technology, Department of Applied Physics and Mechanical Engineering Division of Engineering Materials, 2006.
22. G. W. Meetham, The Development of Gas Turbine Materials, Applied Science Publishers LTD, London, 1981.
23. L. Chapman, *Application of high temperature DSC technique to nickel based superalloys.* Journal of Materials Science, 2004. **39**(24): p. 7229-7236.
24 http://www.msm.cam.ac.uk/phasetrans/2003/Superalloys/superalloys .html.
25. A. Akhtar, S. Hegde and R. C. Reed, *The oxidation of single-crystal nickel-based superalloys.* JOM, 2006. **58**(1): p. 37-42.
26. A. Sato, et al., *On the Mechanical Behavior of a New Single-Crystal Superalloy for Industrial Gas Turbine Applications.* Metallurgical and Materials Transactions A, 2012. **43**(7): p. 2302-2315.
27. http://www.msm.cam.ac.uk/phase-trans/2003/Superalloys/SX/SX.html.
28. V. P. Deodeshmukh, *Hot corrosion behavior of Pt-modified Ni- and Co-based alloys and coatings.* Doctor thesis, Iowa State University, 2007.
29. J. Angenete, K. Stiller and E. Bakchinova, *Microstructural and microchemical development of simple and Pt-modified aluminide diffusion coatings during long term oxidation at 1050°C.* Surface and Coatings Technology, 2004. **176**(3): p. 272-283.
30. J. Angenete, K. Stiller and V. Langer, *Oxidation of Simple and Pt-Modified Aluminide Diffusion Coatings on Ni-based Superalloys-I. Oxide Scale Microstructure.* Oxidation of Metals, 2003. **60**(1-2): p. 47-82.
31. J. Angenete and K. Stiller, *Comparison of inward and outward grown Pt modified aluminide diffusion coatings on a Ni based single crystal superalloy.* Surface and Coatings Technology, 2002. **150**(2-3): p. 107-118.
32. J. Jedlinski, Solid State Phenomena, 1992. **21-22**: p. 335.
33. H. Svensson, P. Knutsson and K. Stiller, *Formation and Healing of Voids at the Metal/Oxide Interface in NiAl Alloys.* Oxidation of Metals, 2009. **71**(3-4): p. 143-156.
34. V. Deodeshmukh and B. Gleeson, *Effects of Platinum on the Hot Corrosion Behavior of Hf-Modified γ'-Ni3Al + γ-Ni-Based Alloys.* Oxidation of Metals, 2011. **76**(1-2): p. 43-55.
35. M. J. Pomeroy, *Coatings for gas turbine materials and long term stability issues.* Materials & Design, 2005. **26**(3): p. 223-231.
36. H. Lai, P. Knutsson and K. Stiller, *The influence of platinum on the oxidation and sodium sulfate induced hot corrosion of NiAl diffusion coatings.* Materials at High Temperatures, 2011. **28**(4): p. 302-308.
37. J. G. Smeggil, A. W. Funkenbusch and N. S. Bornstein, *A Relationship between Indigenous Impurity Elements and Protective Oxide Scale Adherence Characteristics.* Metallurgical Transactions A, June 1986. **17A**: p. 923-932.
38. J. Smialek, *Maintaining adhesion of protective Al2O3 scales.* JOM, 2000. **52**(1): p. 22-25.
39. P. Hou and J. Stringer, *Oxide scale adhesion and impurity segregation at the scale/metal interface.* Oxidation of Metals, 1992. **38**(5-6): p. 323-345.

40. J. Smialek, *Effect of sulfur removal on Al_2O_3 scale adhesion.* Metallurgical Transactions A, 1991. **22**(3): p. 739-752.
41. J. Smialek, *The Effect of Hydrogen Annealing on the Impurity Content of Alumina-Forming Alloys.* Oxidation of Metals, 2001. **55**(1-2): p. 75-86.
42. D. A. Jones, *Principles and Prevention of Corrosion.* Englewood Cliffs, N. J. : Prentice Hall, cop., 1996.
43. P. Kofstad, *High temperature corrosion.* Elsevier Science Publishing CO. INC. N. Y., 1988.
44. N. Birks, G. H. Meier and F. S. Pettit, *Introduction to the high temperature oxidation of metals.* Cambridge University Press, U. K., 2004.
45. Young, D., *High Temperature Oxidation and Corrosion of Metals.* Oxford, U. K., 2008. **1**.
46. http://events.nace.org/library/corrosion/HotCorrosion/Kinetics.asp.
47. G. F. Chen and H. Y. Lou, *Predicting the oxide formation of Ni–Cr–Al alloys with nano-sized grain.* Materials Letters, 2000. **45**(5): p. 286-291.
48. H. Götlind, et al., *The Effect of Water Vapor on the Initial Stages of Oxidation of the FeCrAl Alloy Kanthal AF at 900 °C.* Oxidation of Metals, 2007. **67**(5): p. 251-266.
49. H. Asteman, et al., *Influence of Water Vapor and Flow Rate on the High-Temperature Oxidation of 304L; Effect of Chromium Oxide Hydroxide Evaporation.* Oxidation of Metals, 2000. **54**(1): p. 11-26.
50. H. Asteman, K. S., J.-E. Svensson and L.-G. Johansson, *The influence of water vapor on the corrosion of chromia-forming steels.* Materials Science Forum, 2001. **369-372**: p. 277-286.
51. H. Asteman, J. -E. Svensson and L. -G. Johansson, *Effect of water-vapor-induced Cr vaporizaion on the oxidation of austenitic stainless steels at 700 and 900°C.* Journal of the Electrochemical Society, 2004. **151(3)**: p. 141-150.
52. B. Pujilaksono, et al., *Oxidation of Binary FeCr Alloys (Fe–2.25Cr, Fe–10Cr, Fe–18Cr and Fe–25Cr) in O_2 and in $O_2 + H_2O$ Environment at 600 °C.* Oxidation of Metals, 2011. **75**(3-4): p. 183-207.
53. M. A. Smith, W. E. Frazier and B. A. Pregger, *Effect of sulfur on the cyclic oxidation behavior of a single crystalline, nickel-base superalloy.* Materials Science and Engineering: A, 1995. **203**(1–2): p. 388-398.
54. J. Meier, etc., *High temperature oxidation.* Superalloys II, 1987.
55. C. Luthra, Metall. Trans., 1988. **19A**.
56. I. Levin and D. Brandon, *Metastable Alumina Polymorphs: Crystal Structures and Transition Sequences.* Journal of the American Ceramic Society, 1998. **81**(8): p. 1995-2012.
57. J. Doychak, J. L. Smialek and T. E. Mitchell, *Transient oxidation of single-crystal β-NiAl,* Metallurgical Transactions A, 1989. **20A**: p. 499-518.
58. G. C. Rybicki and J. L. Smialek, *Effect of the θ - α-Al_2O_3 transformation on the oxidation behavior of β-NiAl + Zr.* Oxidation of Metals, 1989. **31**(3): p. 275-304.
59. H. Svensson, *Initial oxidation of β-NiAl(Pt) coatings and model alloys* Phd thesis, 2006.
60. J. Alvarado-Orozco, et al., *First Stages of Oxidation of Pt-Modified Nickel Aluminide Bond Coat Systems at Low Oxygen Partial Pressure.* Oxidation of Metals, 2012, p. 1-16.

61. N. Eliaz, G. Shemesh and R. M. Latanision, *Hot corrosion in gas turbine components.* Engineering Failure Analysis, 2002. **9**(1): p. 31-43.
62. T. S. Sidhu, S. Prakash and R. D. Agrawal, *Hot corrosion and performance of nickel-based coatings.* Current Science, 2006. **90**: p. No.1.
63. J. A. Goebel and F. S. Pettit, *Na_2SO_4-induced accelerated oxidation(hot corrosion) of nickel.* metall trans, 1970. **1**: p. 1943-54.
64. J. A. Goebel and F. S. Pettit, *The influence of sulfides on the oxidation behavior of nickel-base alloys.* Metal Trans, 1970. **1**: p. 3421-9.
65. P. Knutsson, H. Lai and K. Stiller, *A method for investigation of hot corrosion by gaseous Na_2SO_4.* Corrosion Science, 2013. **73**: p. 230-236.
66. J. A. Goebel, F. S. Petit and G. W. Goward, *Mechanisms for the hot corrosion of nickel-base alloys.* Metallurgical transactions, 1973. **4**: p. 261-278.
67. S. Mrowec, *The problem of sulfur in high-temperature corrosion.* Oxidation of Metals, 1995. **44**(1-2): p. 177-209.
68. X. Liu and B. Gleeson, *The Effect of Environmental Sulfur on the Establishment and Structural Stability of Alumina Scales.* Oxidation of Metals, 2013. **80**(5-6): p. 517-527.
69. G. Luckman and R. S. Polizzotti, *An effect of chemisorbing surface reaction poisons on the transition from internal to external oxidation.* Metallurgical and Materials Transactions A, 1985. **16(1)**: p. 133-136.
70. A. Järdnäs, J. -E. Svensson, and L. -G. Johansson, *The Inhibitive Effect of Traces of SO_2 on the Oxidation of Iron.* Oxidation of Metals, 2003. **60**(5-6): p. 427-445.
71. V. Pecharsky and P. Zavalij, Fundamentals of Powder Diffraction and Structural Characterization of Materials Springer Science-Business Media, New York: 2005.
72. D. J. Stokes, Principles and practice of variable pressure/environmental scanning electron microscopy. John Wiley & Sons Ltd, U. K., second edition: 1997.
73. J. Li, *The focused-ion-beam microscope more than a precision ion milling machine.* Journal of the Minerals, Metals and Materials Society, March 2006. **58**: p. 27-31.
74. http://www.globalsino.com/EM/page3891.html.
75. D. B. Williams and C. B. Carter, Transmission Electron Microscopy**:** imaging, Springer Science + Business Media, Second Edition: 2009. **3**: p. 371.
76. W. Zhou, et al., *Scanning Microscopy for Nanotechnology: Techniques and Applications.* Springer Science, 2006.
77. http://www.asminternational.org/documents/10192/1887769/amp16205p034.pdf/df7124af-e021-43a5-9863-3d35aaf21f8a.
78. http://www.ebsd.com/index.php/ebsd-explained/introduction-to-ebsd.
79. http://www.oxford-instruments.com/products/microanalysis/ebsd.
80. H. Svensson, et al., *Influence of Pt on the metal–oxide interface during high temperature oxidation of NiAl bulk materials.* Corrosion Science, 2009. **51**(3): p. 539-546.
81. H. Lai, et al., *High Temperature Corrosion of Ni-Based Alloys SCA425+ and IN792.* Oxidation of Metals, 2013. **80**(5-6): p. 505-516.

82. M. Paneru, et al., *Corrosion Mechanism of Alloy 310 Austenitic Steel beneath NaCl Deposit under Varying SO_2 Concentrations in an Oxy-fuel Combustion Atmosphere.* Energy & Fuels, 2013. **27**(10): p. 5699-5705.
83. S. Karlsson, et al., *KCl-Induced High Temperature Corrosion of the Austenitic Stainless Steel 304L–The Influence of SO_2.* Materials Science Forum, September, 2011. **696**: p. 224-229.
84. N. Mu, K. Jung, M. N. Yanar, et al, *The Effects of Water Vapor and Hydrogen on the High-Temperature Oxidation of Alloys.* Oxidation of Metals, June 2013. **79**: p. 461-472.
85. A. Skilbred and R. Haugsrud, *The Effect of Water Vapour on the Corrosion of Sandvik Sanergy HT Under Dual Atmosphere Conditions.* Oxidation of Metals, 2013. **79**(5-6): p. 639-654.
86. S. R. J. Saunders, M. Monteiro and F. Rizzo, *The oxidation behaviour of metals and alloys at high temperatures in atmospheres containing water vapour: A review.* Progress in Materials Science, 2008. **53**(5): p. 775-837.
87. A. Järdnäs, J. -E. Svensson and L. -G. Johansson, *Influence of SO_2 on the Oxidation of 304L Steel in O_2 + 40%H_2O at 600 °C.* Oxidation of Metals, 2008. **69**(3-4): p. 249-263.